JOURNAL OF GEOPHYSICAL RESEARCH, VOL. 103, NO. D15, PAGES 18,927–18,946, AUGUST 20, 1998

Meteorological factors associated with inhomogeneous ozone concentrations within the Mexico City basin

Jerome D. Fast and Shiyuan Zhong

Pacific Northwest National Laboratory, Richland, Washington

Abstract. Meteorological processes associated with inhomogeneous ozone concentrations over Mexico City are examined by using observations from a recent field campaign and a mesoscale dynamics and dispersion modeling system. During this 4-week field campaign, meteorological measurements of the spatial flow structure within the Mexico City basin were obtained for the first time. A mesoscale model that employs four-dimensional data assimilation is used to create analyses that describe the boundary layer characteristics and local and regional circulations in the vicinity of Mexico City. The mesoscale analyses are then used to drive a Lagrangian particle dispersion model to simulate pollutant transport and diffusion. The resemblance between the calculated particle concentration fields and the observed spatial ozone patterns indicates that the mesoscale analyses, based on the model and the observed profiles of wind, temperature, and humidity, captured the main flow features responsible for the inhomogeneous ozone concentrations within the basin. The highest particle concentrations usually occurred in the vicinity of the peak ozone concentrations during the afternoon. The observations and mesoscale analyses provided evidence that the circulations are highly complex, and relatively weak upper level synoptic systems had an impact on the local and regional thermally driven flows in the area. In addition to horizontal advection and vertical diffusion, vertical wind shears, recirculation patterns associated with venting and entrainment processes, and mean vertical motions due to convergence within the basin also played an important role in producing the spatial variations in the near-surface particle distributions. The contribution of emissions from the previous day was found to be relatively minor for the periods examined in this study, even though the nocturnal wind speeds were light, suggesting that the high ozone concentrations are not due to multiday accumulation of pollutants.

1. Introduction

The rapid growth of megacities has led to serious urban air pollution problems in many developing countries. For example, hourly averaged ozone concentrations in the Mexico City Metropolitan Area (MCMA) exceed the Mexican air quality standard of 110 ppb nearly every day and often exceed twice the standard. Ozone concentrations as high as 441 ppb have been measured during the most severe air pollution events [*Garfias and Gonzolas*, 1992]. In contrast to midlatitude megacities, ozone exceedances can occur at any time during the entire year because the subtropical latitude (~19.4°N) and high altitude (~2250 m mean sea level, or msl) are conducive to ozone production during the winter as well as the summer. The prevailing dry, clear-sky conditions during the winter months lead to the formation of strong surface-based inversions at night [*Collins and Scott*, 1993; *Garfias and González*, 1992] that persist for several hours following sunrise. Strong solar heating of the ground generates turbulent mixing that erodes these inversions in the morning, producing deep boundary layers by the afternoon. Pollutants initially trapped below the inversion are then mixed within the convective boundary layer (CBL), which can be as high as 4 km above the ground. There is sufficient time for the photochemical production of ozone in the morning, before the development of the deep CBL, because of high emission rates and intense subtropical high-altitude solar radiation. During the wet summer season, clouds inhibit photochemistry, and precipitation removes trace gases and particulates so that extremely high ozone episodes are less frequent.

Since the city is located within an elevated basin, it is thought that the mountain ranges tend to restrict pollutant ventilation. The effect of the surrounding terrain on the development of thermally driven flows has been observed [*Jauregui*, 1988; *Lauer and Klaus*, 1975], but few routine meteorological measurements are made in the region that can be used to describe the influence of local and regional circulations on pollutant transport. For example, the twice-daily rawinsondes at the airport are the only routine upper air measurements. Hourly near-surface measurements of wind speed, direction, temperature, and humidity are made at a number of locations throughout the city, but some of the observations are not representative of the surrounding conditions, since they are affected by nearby buildings and trees in the urban environment. These operational upper air and surface observations are insufficient to describe conditions within the basin when the winds are light and variable or when multiscale flow interactions form complicated circulations.

Additional instrumentation has been deployed during a recent field campaign to better describe the meteorological and air chemistry characteristics over the MCMA. Over a 3-week period in February 1991, rawinsonde, tethersonde,

Paper number 98JD01725.
0148-0227/98/98JD-01725$09.00

and aircraft measurements [*Nickerson et al.*, 1992] were made as part of the Mexico City Air Quality Research Initiative (MARI) to provide input data for air quality models [*Streit and Guzmán*, 1996]. Most of the meteorological measurements were made at one site, and information regarding the spatial wind field characteristics was obtained only on a few days. *Bossert* [1997], *Wellens et al.* [1994], and *Williams et al.* [1995] used data from the 1991 MARI field campaign to evaluate the local circulations produced by mesoscale models and the transport of pollutants simulated by dispersion models. *Bossert* [1997] demonstrated that both regional- and synoptic-scale meteorology are important for understanding flows and dispersion within the Mexico City basin.

Ozone measurements made throughout the MCMA over the past several years have shown that ozone concentrations are usually highest in the southwest section of the city and lowest in the northeast [*Bian et al.*, 1998; *Bravo et al.*, 1996; *Collins and Scott*, 1993; *Streit and Guzmán*, 1996]. Climatological analyses suggest that the dominant near-surface northerly winds during the day transport pollutants to the south; however, the winds and ozone concentrations associated with individual pollution episodes imply a more complex relationship. For example, vertical wind shears can effectively disperse pollutants over a much larger area than can near-surface advection and diffusion alone. Preliminary modeling studies [*Fast et al.*, 1997; *Zhong et al.*, 1997] have shown that the interaction of synoptic flows and local thermally driven circulations may determine where the highest pollutant concentrations occur within the basin. Because of the lack of routine meteorological and air chemistry measurements aloft over the city, the effect of the time-dependent three-dimensional wind field on pollutant distribution within the basin is not well understood. Even though 80% of the air pollution in Mexico City has been attributed to vehicle emissions [*Collins and Scott*, 1993], it is likely that the distribution of point sources, such as the industrial emission sources located in the northern end of the city [*Fuentes-Gea and Garcia-Gutierrez*, 1990], plays a role in producing spatially inhomogeneous pollutant concentrations.

A detailed spatial and temporal description of the complex circulations within the basin is required to adequately describe pollutant transport and diffusion over Mexico City. In this study a mesoscale model that employs four-dimensional data assimilation is used to simulate small-scale and regional circulations influenced by complex terrain within and around the basin during 7 high-ozone days of a field campaign conducted in February and March 1997. The mesoscale model results are coupled to a Lagrangian particle dispersion model to identify the meteorological mechanisms that contribute to the observed spatial ozone concentration variations over Mexico City. This approach was found to be very useful in describing the atmospheric processes responsible for the ozone layers observed during the 1993 North Atlantic Regional Experiment [*Fast and Berkowitz*, 1996; *Doran et al.*, 1996] and the 1995 North American Research Strategy for Tropospheric Ozone field campaign [*Berkowitz et al.*, 1998]. Since aircraft measurements [*Nickerson et al.*, 1992, 1993] have suggested that pollutant layers may persist over Mexico City from one day to the next, the particle dispersion model is also used to estimate the relative contribution of previous day emissions on concentrations within the basin atmosphere.

2. The 1997 Field Campaign

As part of the Investigacion sobre Materia Particulada y Deterioro Atmosférico-Aerosol and Visibility Evaluation Research (IMADA-AVER) project a meteorological field campaign (Doran et al., 1998) was conducted between February 24 and March 22, 1997, to provide essential information about the boundary-layer structure and evolution in the vicinity of Mexico City. IMADA-AVER was conducted cooperatively by the U.S. Department of Energy and the Instituto Mexicano del Petroleo. The objectives of the IMADA-AVER project were to understand the nature and causes of the observed high particulate concentrations, high ozone concentrations, and visibility impairment in the region. In this study we focus on the meteorological processes that contribute to spatial variations of high ozone concentrations within the basin.

2.1. Instrumentation

During the field campaign, hourly vertical wind profiles within 4 km of the ground were obtained from four 915-MHz radar profilers located at Cuautitlan, Teotihuacan, UNAM, and Chalco (Figure 1). A comparison of horizontal wind component measurements from rawinsondes and wind profilers over a 2-year period have been shown by *Weber and*

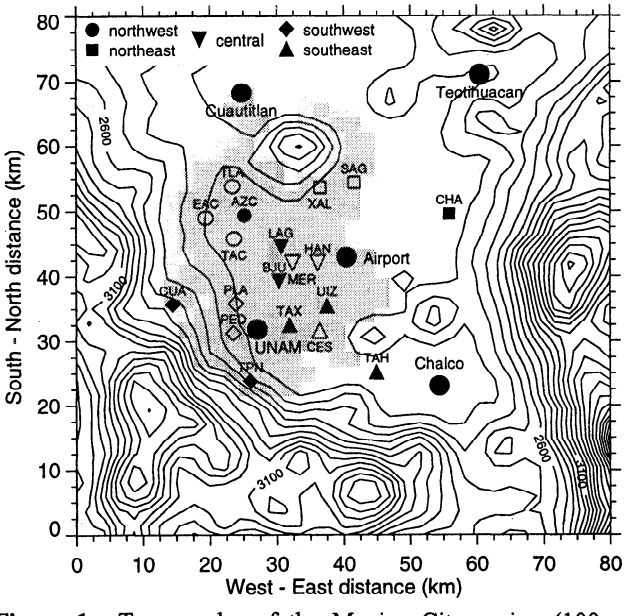

Figure 1. Topography of the Mexico City region (100-m contour interval), locations of radar wind profilers and radiosondes during the 1997 IMADA-AVER field campaign (Cuautitlan, Teotihuacan, UNAM, and Chalco), and locations of the RAMA monitoring stations that measure near-surface ozone. The symbols denote station groups; open symbols denote stations that also measure meteorological quantities. Gray shading denotes the MCMA. Surface monitoring stations include Tlalnepantla (TLA), ENEP-Acatlan (EAC), Azcapotzalco (AZC), Tacuba (TAC), Xalostoc (XAL), San Agustin (SAG), Chapingo (CHA), Lagunilla (LAG), Merced (MER), Hangares (HAN), Benito Juarez (BJU), Cuajimalpa (CUA), Plateros (PLA), Pedregal (PED), Tlalpan (TPN), Taxquena (TAX), UAM-Iztapalapa (UIZ), Cerro de la Estrella (CES), and Tlahuac (TAH).

Wuertz [1990] to have differences with a standard deviation of about 2.5 m s^{-1} that are mainly due to meteorological variability in the wind. Temperature and humidity profiles were obtained from radiosondes launched 5 times per day (0800, 1100, 1330, 1630, and 1930 local standard time, or LST) at the same locations. Twice-daily rawinsonde soundings were made at the Mexico City airport near the middle of the basin. Additional temperature and humidity profiles were obtained from radiosondes launched at Tres Marias (1330 and 1630 LST), located about 45 km southeast of Mexico City, and Pachuca (1330, 1630, and 1830 LST), located about 70 km northeast of Mexico City. In contrast to the 1991 MARI field campaign, meteorological instrumentation was deployed at several locations to obtain continuous information about the spatial characteristics of the wind, temperature, and humidity.

Air quality data were provided by an automated surface network of 33 monitoring stations in and surrounding Mexico City. This network, called the Red Automática de Monitoreo Atmosférico (RAMA), routinely provides hourly near-surface measurements of various pollutants. Ozone, carbon monoxide, sulfur dioxide, nitrogen oxides, and particulates are among the quantities measured at RAMA monitoring stations. The instrumentation at the RAMA stations follows the U.S. Environmental Protection Agency guidelines [*Raga and Le Moyne*, 1996]. The locations of the 19 monitoring stations that measure ozone are shown in Figure 1. The RAMA stations are grouped into five geographic regions, northwest, northeast, southwest, southeast, and central, to obtain average ozone concentrations over regions of the MCMA. Near-surface wind speed, direction, temperature, and humidity are measured at 10 of these locations, denoted by the open symbols in Figure 1. During the field experiment, additional surface meteorological stations measured the wind speed and direction, temperature, humidity, and solar radiation at a height of 2 m at the Teotihuacan and UNAM sites and at a height of 10 m at the Chalco site.

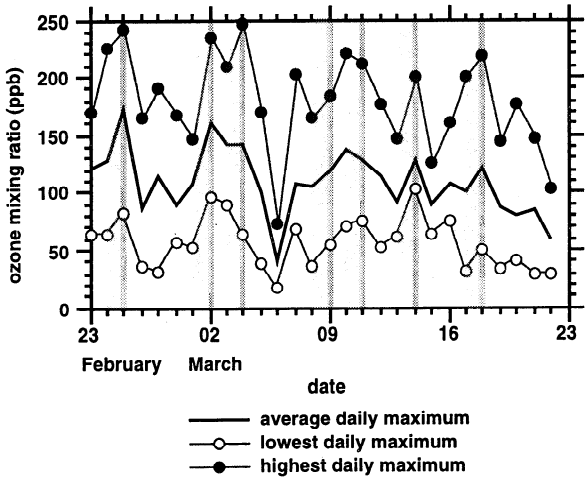

Figure 2. Daily maximum hourly ozone concentration (heavy line) averaged over the 19 RAMA stations and the highest and lowest daily maximum values during the field campaign. The vertical gray lines denote days examined in this study.

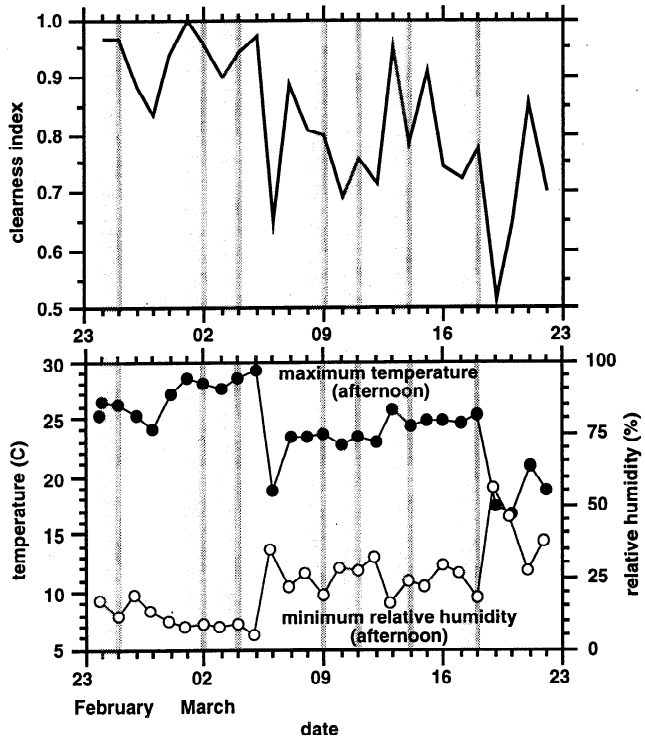

Figure 3. Meteorological quantities measured during the field campaign at the UNAM surface station including the clearness index (see text for details), daily maximum temperature, and daily minimum relative humidity. The vertical gray lines denote days examined in this study.

2.2. Observations

The temporal variation of the basin-averaged daily maximum ozone concentrations and the highest and lowest ozone concentrations observed among the stations during the field campaign are given in Figure 2. The Mexican ozone standard of 110 ppb was exceeded nearly every day at one or more stations, and there were 11 days on which hourly ozone concentrations exceeded 200 ppb. Daily maximum ozone concentrations varied among the individual stations by as much as 150 ppb on a given day, demonstrating the spatial inhomogeneity of ozone within the basin. The gray lines in Figure 2 denote 7 days that have been chosen for model simulations, as we will describe in section 3.3. These periods were chosen because of the relatively high values and differing spatial distributions of ozone concentrations.

As Figure 2 shows, the lowest ozone concentration occurred on March 6, the highest ozone episodes occurred before March 6, and more high-ozone days occurred before March 6 than during the period afterward. The daily ozone values appear to be associated with the ambient meteorological conditions. For example, the cloudiness, temperatures, and humidities at UNAM depicted in Figure 3 were distinctly different before and after March 6. The clearness index given in this figure is a function of the daily integrated solar radiation. A value of 1 represents clear skies between sunrise and sunset, and smaller values are produced with increased cloudiness. Before March 6 the clearness index often exceeded 0.9, the maximum temperatures were usually between 25° and 30°C, and the afternoon relative humidities

were less than 20%. After March 6 the skies became partly to mostly cloudy, the temperatures were lower, and the relative humidities were higher. The higher ozone concentrations were associated with the clear skies, warm temperatures, and dry conditions early in the field experiment.

As we mentioned previously, ozone concentrations varied significantly across the basin and exhibited significant day-to-day variations (Figure 2). Typical spatial and temporal variations are shown by the hourly surface ozone concentrations averaged over each station group in Figure 4. The average ozone concentrations on February 25 (Figure 4a) were the highest recorded during the field campaign. Ozone concentrations exceeded 110 ppb at all of the stations during the afternoon, but the center and western stations were about 50 ppb higher than the eastern stations. Ozone concentrations on March 2 (Figure 4b) were highest in the southwest at 1300 LST; however, maximum values were observed at the northwest stations later in the afternoon at 1700 LST. The maximum ozone concentrations occurred in the southeast on March 4 and 18 (Figures 4c and 4f) and in the northwest on March 11 and 14 (Figures 4d and 4e). NO_x concentrations also exhibited spatial inhomogeneity and typically reached peak values of 200 to 300 ppb between 0800 and 0900 LST, suggesting that vehicular emissions were large contributors to ozone production. The region with the highest NO_x concentrations did not necessarily correspond to the region with the highest ozone values, indicating that ozone distribution is a function of transport processes, the timing of the emissions, and the rates at which NO_x and reactive hydrocarbons are transformed into secondary pollutants by photochemical reactions.

The spatial ozone variations shown in Figure 4 suggest that the basin circulations were significantly different from one day to the next. Subtle changes in the ambient flow, due to day-to-day variations in the large-scale synoptic conditions, are expected to affect the development of thermally driven flows produced by local and regional topographic variations. High-pressure systems and weak upper-level winds characterize the synoptic conditions over central Mexico in the winter; however, the propagation of troughs and low-pressure systems over the United States affected the upper-level flow over central Mexico several times during the field campaign as shown in Figure 5. Relatively large pressure gradients and wind speeds at the 500-hPa level occurred over central Mexico on March 2 (Figure 5a) as a result of a cutoff low over Texas. Weak pressure gradients were observed on March 4 (Figure 5b) and 14 (Figure 5c), but the position of the troughs over the United States produced different wind directions over central Mexico on each day. Wind profiler measurements indicated that even weak synoptic forcing affected the thermally driven wind systems so that it was difficult to characterize common near-surface flow features within the basin during the field campaign [*Doran et al.*, 1998].

While the wind profiler network provided valuable information about the spatial characteristics of the winds, they were insufficient to fully describe details of the three-dimensional flows within the basin that affect pollutant transport. Prognostic mesoscale models are the only tools available that can be used to obtain realistic flow characteristics in data sparse regions, such as the center of the basin and the mountainous regions surrounding the city.

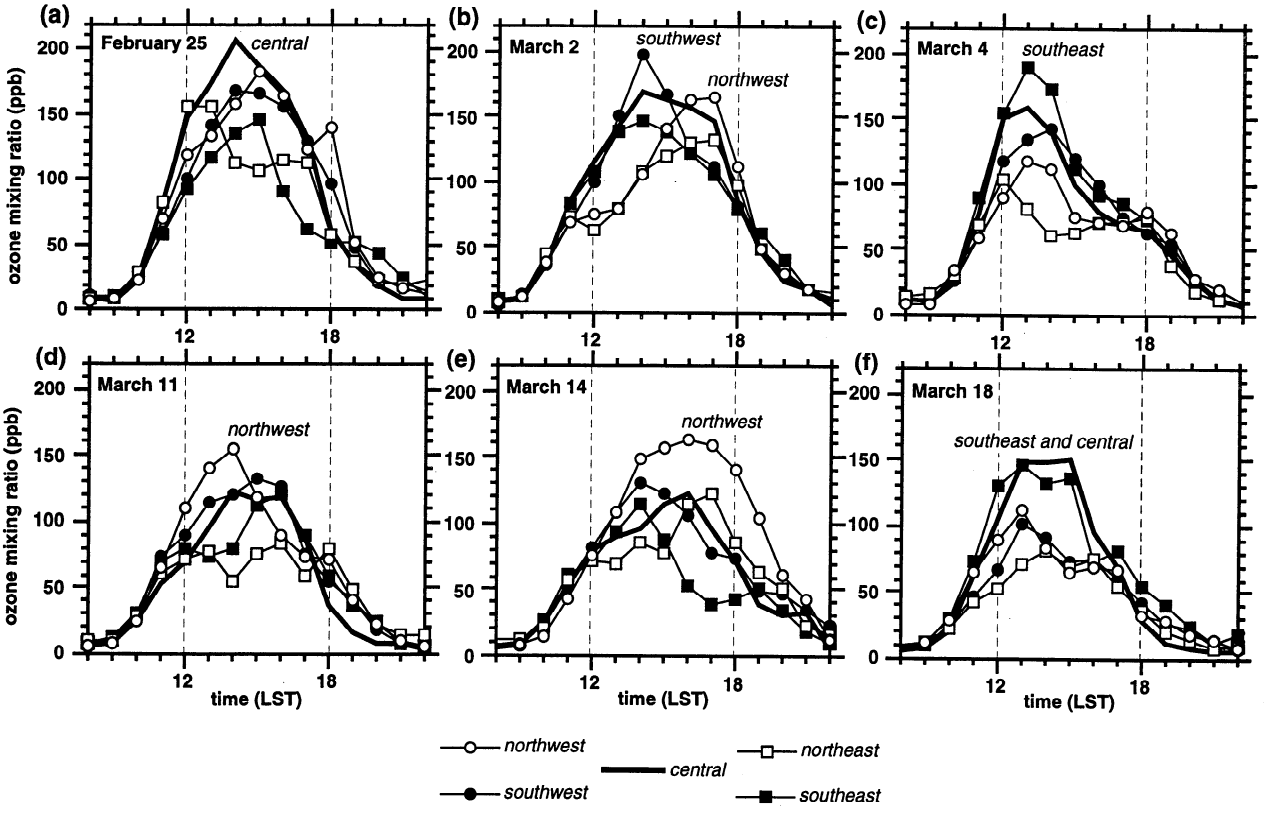

Figure 4. Hourly surface ozone concentrations averaged over each station group for (a) February 25, (b) March 2, (c) March 4, (d) March 11, (e) March 14, and (f) March 18, 1997.

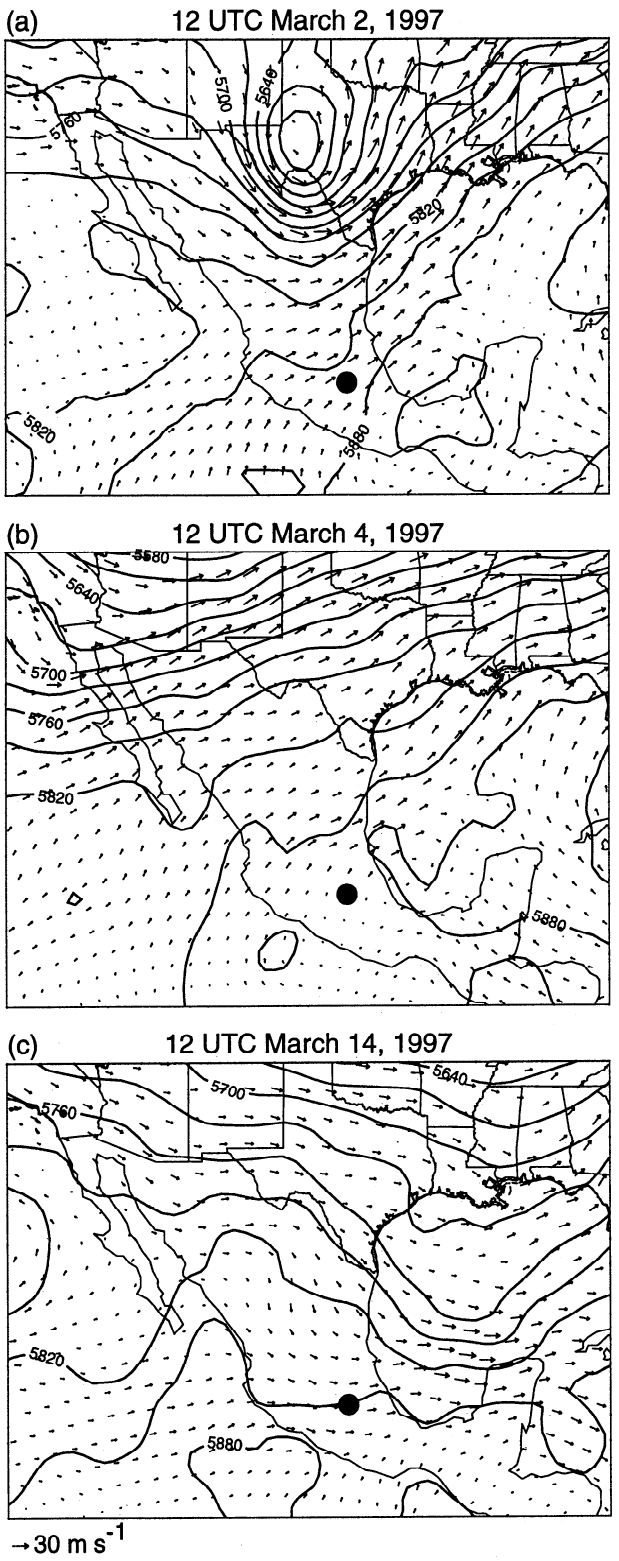

Figure 5. The 500-hPa geopotential heights and winds at 1200 UTC from the NCEP AVN model analyses on (a) March 2, (b) March 4, and (c) March 14. The solid circle denotes the location of Mexico City.

3. Model Description

A mesoscale dynamic and dispersion modeling system is used to investigate the effect of local and regional thermally driven flows on the spatial distribution of ozone within the basin. We employ both observations from the 1997 field campaign and mesoscale model results to identify the meteorological processes in the vicinity of the MCMA.

3.1. Atmospheric Mesoscale Model

The Regional Atmospheric Modeling System (RAMS) [*Pielke et al.*, 1992] is the mesoscale meteorological model used to describe the meteorological conditions in the vicinity of Mexico City. The turbulence parameterization consists of a simplified second-order closure method that employs a level 2 diagnostic scheme or a level-2.5 scheme with a prognostic turbulence kinetic energy equation [*Mellor and Yamada*, 1982; *Helfand and Labraga*, 1988]. Although the cumulus and microphysics parameterizations are not activated to produce precipitation, condensation of vapor to cloud water occurs in areas of supersaturation. The *Chen and Cotton* [1983] shortwave and longwave parameterizations are used to determine the heating or cooling caused by radiative flux divergences. Turbulent sensible heat, latent heat, and momentum fluxes in the surface layer are based on similarity equations [*Louis*, 1979]. Prognostic soil-vegetation relationships are used to calculate the diurnal variations of temperature and moisture at the ground-atmosphere interface. In this study, vegetation type is based on a U.S. Geological Survey 1-km data set for North America. Vegetation in the Mexico City region consists of forests at the higher elevations surrounding the city and grass, crops, and shrubs at the lower elevations.

RAMS employs a terrain-following coordinate system and a two-way interactive nested grid structure. As Figure 6 shows, the modeling domain consists of three nested grids with horizontal grid spacings of 36, 9, and 2.25 km. The outer grid encompasses most of Mexico and parts of the Gulf of Mexico and Pacific Ocean. The inner grid encompasses the Mexico City basin and the surrounding mountain ranges. By employing a nested grid configuration the effects of synoptic and regional-scale flows on local circulations within the basin can be represented. A stretched terrain-following coordinate is employed with a grid spacing of 50 m adjacent to the surface. The grid spacing is 100 m between 50 and 1250 m above ground level (AGL); above this height the spacing gradually increases to 1500 m near the model top at an elevation of 17.8 km AGL. Because of the staggered coordinate system the lowest model coordinate is at about 26 m AGL. There are 42 vertical levels. With this vertical resolution, 26 grid points are positioned within 4 km of the ground to resolve boundary-layer processes responsible for pollutant transport from surface releases.

A nudging four-dimensional data assimilation (FDDA) technique has been incorporated into RAMS [*Fast*, 1995; *Harms et al.*, 1992], using a tendency term that is added to the prognostic equations of the model. In this study, FDDA brings four prognostic variables (u and v component of the wind, potential temperature, and specific humidity) into closer agreement with the standard upper air soundings at the Mexico City airport (0000 and 1200 UTC periods), the hourly wind profiler data, and the radiosondes (five per day) at the four primary sites (Cuautitlan, Teotihuacan, UNAM, and Chalco) throughout the simulation period within the inner grid. On grids 1 and 2, data from the 0000 and 1200 UTC rawinsondes are incorporated into the model. Surface observations are not assimilated into the model analyses. The

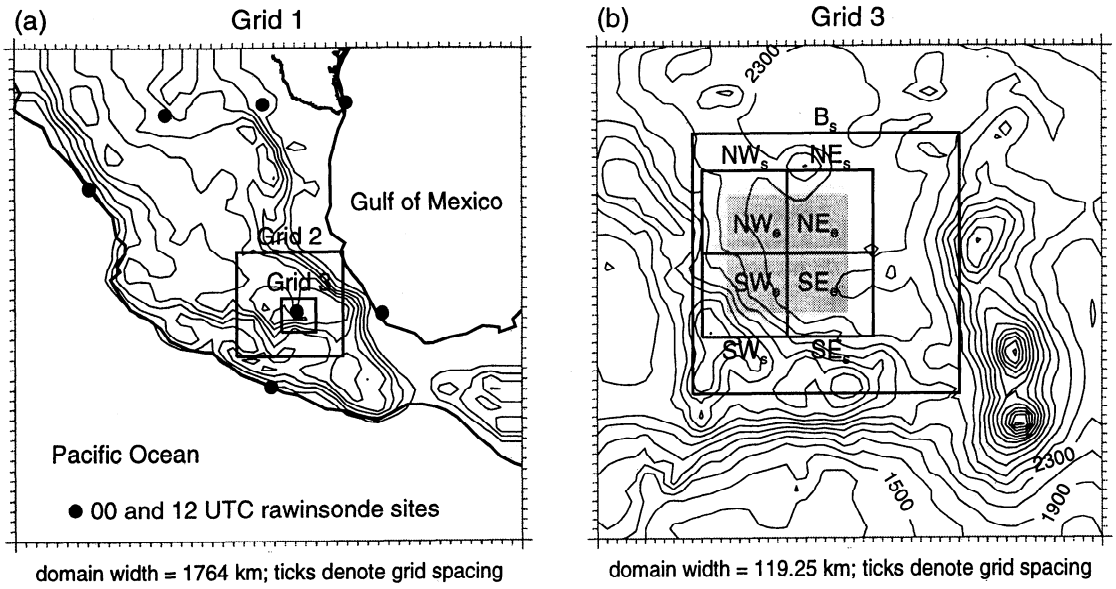

Figure 6. Grid location and topography employed by the mesoscale model on (a) grid 1 and (b) grid 3, four area emission sources employed by the particle dispersion model denoted by gray boxes SW_e, SE_e, NW_e, and NE_e, and five particle sampling domains denoted by SW_s, SE_s, NW_s, NE_s, and B_s.

resulting meteorological fields are mesoscale analyses, which combine the predicted and observed variables when and where observations are available. FDDA is applied to limit the forecast errors in the prognostic variables and to reduce the uncertainties associated with pollutant transport. Additional details of the FDDA procedure are given in the appendix.

3.2. Lagrangian Particle Dispersion Model

A Lagrangian particle dispersion model [*Fast*, 1995] is used to examine the transport characteristics associated with meteorological processes in the vicinity of the MCMA. Dispersion is simulated by tracking a large number of particles based on the mean velocity components predicted by RAMS and subgrid-scale turbulent velocity components. The mean velocity fields employed by the model are based on the mesoscale analyses at 1-hour intervals. The model linearly interpolates the mean velocity field in time during individual 1-hour periods using a 15-s time step. The sub-grid scale turbulent velocities are computed by solving the Langevin equation with a Markov chain formulation [*Legg and Raupach*, 1982] that is based on the Thomson formulation of the equation for the turbulent vertical velocity component [*Hurley and Physick*, 1991]. The turbulent velocity statistics are consistent with the second-order closure applied in the mesoscale model. Particles are nonbuoyant, and a perfect reflection of particles occurs at the ground. Each particle is tagged by its release location, release time, and current position so that the history of a particle plume and individual trajectories can be obtained. This information is useful in identifying the atmospheric mechanisms associated with pollutant transport and diffusion.

3.3. Experimental Design

Seven days from the 1997 IMADA-AVER field campaign are examined: February 25 and March 2, 4, 9, 11, 14, and 18. These days are chosen because the peak ozone values occurred in different areas of the MCMA as shown in Figure 4, suggesting that different meteorological processes may have been responsible for the ozone distributions on each day. In contrast to the observations in Figure 4, ozone concentrations on March 9 exhibited only minor spatial variations (not shown).

A mesoscale simulation is performed for each of the seven cases. Each simulation starts at 0600 LST and lasts for 42 hours, with the second afternoon being the period of interest. The main reason the model is initialized at this time is that one of our objectives is to examine the relative contribution of the previous day's emissions to near-surface concentrations. Another advantage of initializing the model on the morning of the previous day is that a continuous and realistic treatment of the diurnal boundary-layer characteristics can be obtained. The model is initialized with the National Center for Environmental Prediction's Aviation (AVN) model analyses (1° spacing) and standard 12 UTC rawinsondes (Figure 6a). The mesoscale model's lateral and top boundary points are forced, through the use of nudging [*Davies*, 1976], toward the AVN objective analysis fields during the simulation period. The forcing at the lateral boundaries is applied on the outermost five grid points of grid 1; the magnitude of the forcing varies linearly in time between 6-hour intervals. Continuous FDDA is applied throughout the simulation period by using data from the field campaign and standard rawinsondes, as we described in section 3.1.

The initial soil and vegetation temperature is set equal to the initial atmospheric temperature at the lowest model grid point. The initial soil moisture is set equal to 25% of the saturation value throughout the soil layer to reflect the dry conditions of the winter season. Soil type is specified as sandy clay loam throughout the domain. Although soil moisture should vary over the domain, there are no reliable data to specify this parameter more accurately. The sea surface temperatures are obtained by interpolating a 2-week composite analysis with a 1° horizontal resolution to the model's ocean grid points. The soil temperature and moisture values at the

lowest soil level and the sea surface temperatures are fixed at their initial values during the simulation period.

Four area emission regions, denoted by the SW_e, SE_e, NW_e, and NE_e gray squares in Figure 6b, are employed by the particle dispersion model. Particles are released randomly within the four sources near the surface between 0600 and 1800 LST on each day of the simulation period by using a constant release rate. The same release rate (28 particles min^{-1}) is used for each source in which particles are emitted every 15 s. More than 160,000 particles are released for each case. The resulting concentration fields on the second day are due to both same-day and previous day releases. Five sampling domains, as shown by the boxes in Figure 6b, are used to determine relative concentration in specific portions of the basin atmosphere. Four of the sampling domains, denoted by SW_s, SE_s, NW_s, and NE_s, are located over the MCMA and are slightly larger than the emission sources. A larger sampling domain, denoted by B_s, encompasses most of the basin.

4. Results

Discussion of the model results will focus on the March 2, 4, and 14 cases, although some features from the other cases will be included as well. Results from these cases are presented because the spatial distribution of ozone was significantly different on each day, suggesting that different circulations may have affected the transport of pollutants within the basin. The temporal and spatial variation of ozone on the other days had characteristics that were similar to those on March 2, 4, and 14. We first present observed and simulated potential temperature and wind profiles to describe the development of the boundary layer over the MCMA. Then the surface wind and particle concentration fields are examined and compared to the observed ozone distributions. The vertical structure of the wind, temperature, and particle concentrations are presented next to illustrate the effect of vertical wind shears on near-surface particle concentrations. Finally, the effects of previous day emissions on concentrations within the basin atmosphere are quantified.

4.1. Observed and Simulated Meteorological Profiles

The observed and simulated potential temperatures at the UNAM site on March 2, 4, and 14 are shown in Figure 7. The 0800 LST profiles were characterized by several layers, including a surface-based inversion, a less stable transition layer, and another strong stable layer aloft. Strong radiative cooling as a result of the dry, clear-sky conditions in the elevated basin led to the development of the near-surface inversions. Surface heating produced only a relatively shallow mixed layer by 1100 LST on each day, implying that pollutants emitted in the morning would be trapped near the surface for a substantial period of time. CBL growth was rapid after 1100 LST on each day, since the atmosphere was

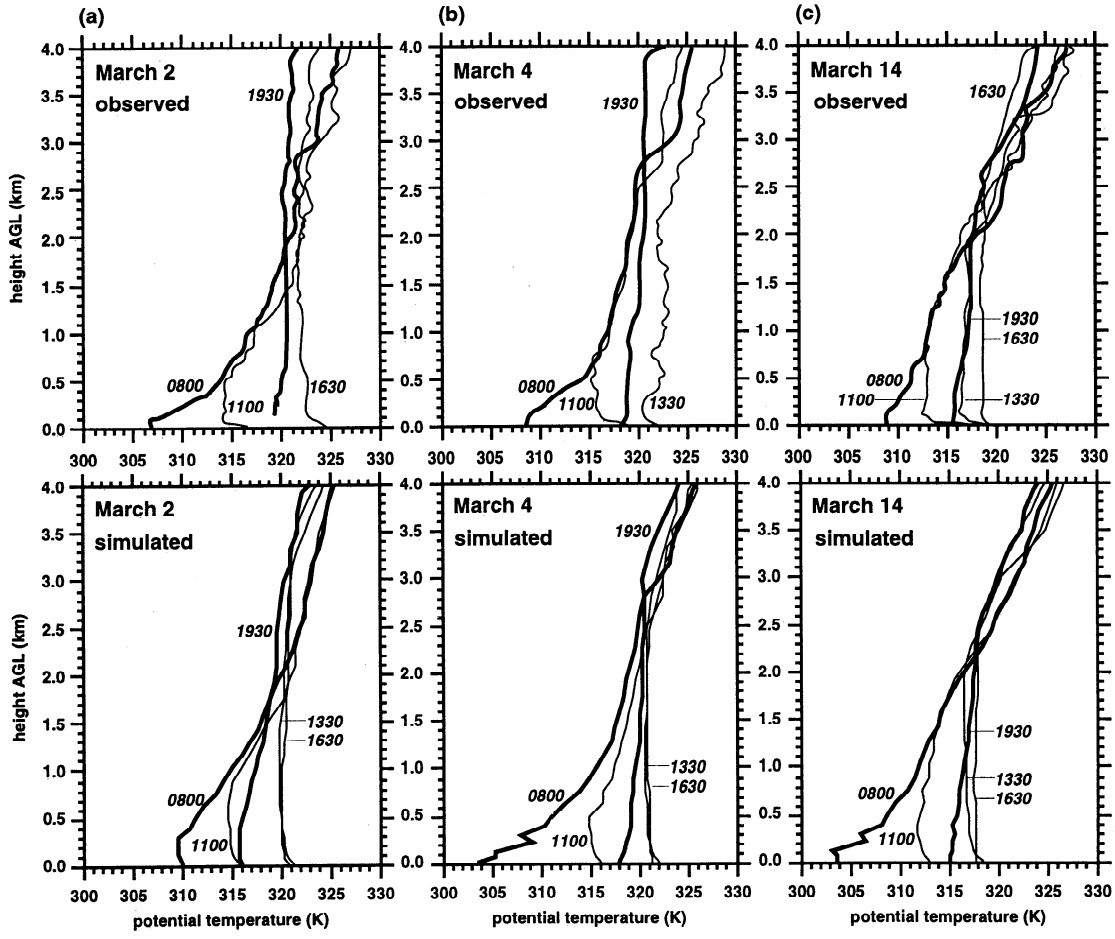

Figure 7. Observed and simulated potential temperature profiles at UNAM for (a) March 2, (b) March 4, and (c) March 14.

less stable aloft. Mixed layer depths late in the afternoon were as high as 4 km AGL on March 2 and 4 and 2.5 km AGL on March 14. The model qualitatively reproduced the features of the observed potential temperature profiles; however, the simulated temperatures within 0.5 km of the surface were 5°C lower than those observed at 0800 LST (except on March 2), even though the radiosonde data were assimilated into the model fields. This decrease also happened at the other three radiosonde sites, indicating the cooling at the surface produced by the model surface energy budget was too strong or the simulated drainage winds that advected cool air down the slopes into the lower basin were too strong. Nevertheless, the simulated temperature profiles were similar to the observed profiles after 1100 LST, so that evolution of the convective boundary layer was adequately simulated by the model.

As we expected, thermally driven flows developed in the region in response to the strong daytime heating in the elevated basin and the presence of deep convective boundary layers in the afternoon. Figure 8 depicts vertical profiles the observed horizontal winds (hourly averaged) and simulated horizontal winds (instantaneous) at UNAM, Cuautitlan, and Chalco sites for March 2, 4 and 14 so that the mesoscale analyses can be directly compared with the observations. The winds at Teotihuacan were often similar to those at Cuautitlan and are therefore not shown. The model qualitatively reproduced most of the observed features, but there were times at which relatively large differences were produced near the surface (see appendix). The gray areas depict the depth of the boundary layer as determined by the model. The top of the boundary layer was defined as either the height where the vertical potential temperature gradient first became larger than 0.0025 K m^{-1} during the day or the height where the turbulent kinetic energy first became smaller than 0.003 m^2s^{-2} during the night.

The winds measured by the profilers between 1 and 3 km AGL (above the average height of the surrounding mountains) indicated the passage of synoptic weather systems. On March 2 (Figure 8a) the winds were westerly at about 10 m s^{-1} until 1500 LST as a result of an upper-level cutoff low over Texas that produced strong synoptic winds above 700 hPa over central Mexico (Figure 5a). The upper-level winds weakened significantly after 1500 LST as the low moved to the east, decreasing the pressure gradient over Mexico. The 500-hPa winds over northern Mexico were southwesterly as a result of a trough over the western United States on March 4 (Figure 5b); however, northeasterly winds between 5 and 10 m s^{-1} were measured above 1.5 km AGL at each profiler over the entire day (Figure 8b). A trough over the Gulf of Mexico (Figure 5c) was responsible for the upper-level westerly winds at about 15 m s^{-1} on March 14 (Figure 8c). The westerly winds observed by the profilers above 2.2 km AGL weakened late in the afternoon as a ridge of high pressure developed over Mexico. A high-pressure system centered over southeastern Mexico at 700 hPa may have been responsible for the southerly winds at about 5 m s^{-1}

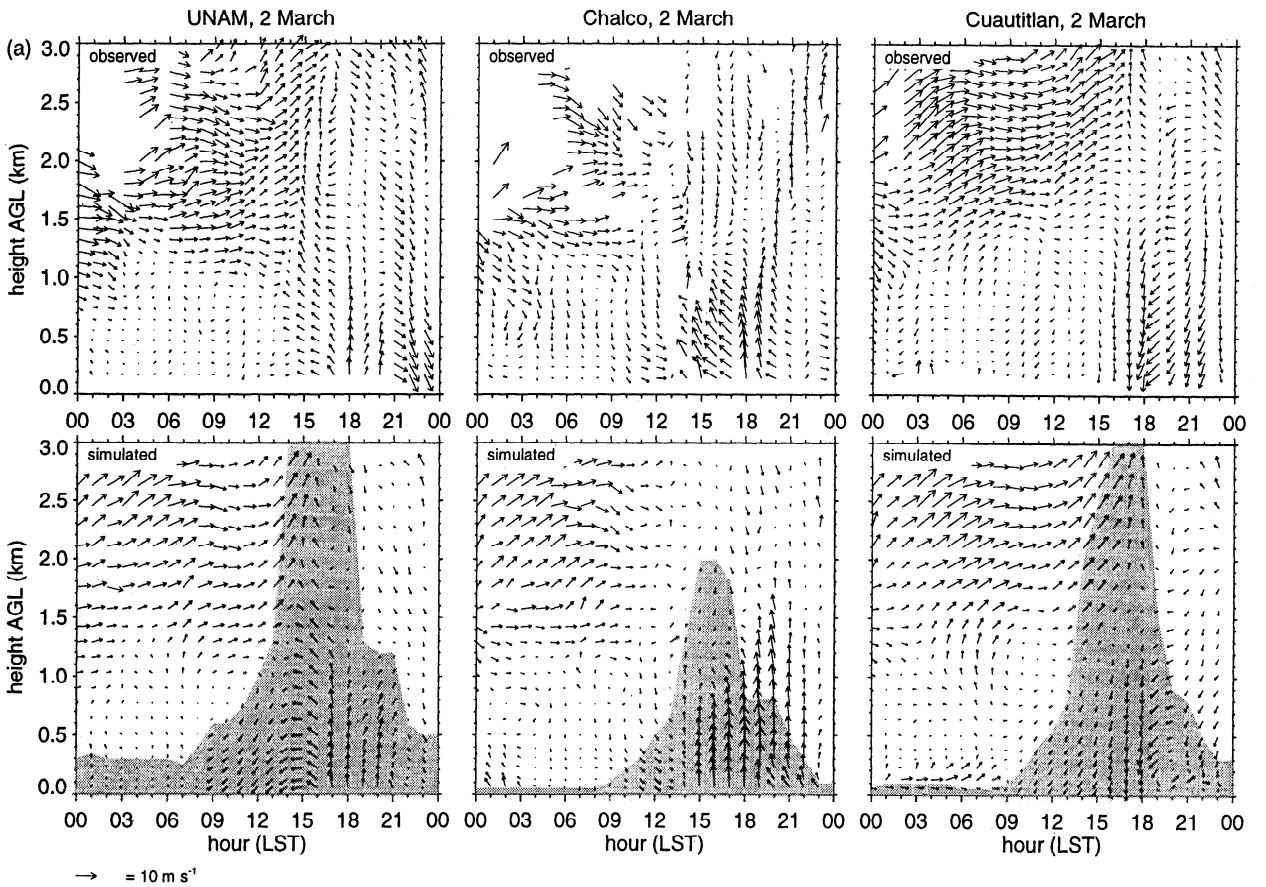

Figure 8. Vertical profiles of the observed and simulated horizontal winds at the UNAM, Chalco, and Cuautitlan sites on (a) March 2, (b) March 4, and (c) March 14, where the gray shading indicates the vertical extent of the simulated boundary layer (see text for details).

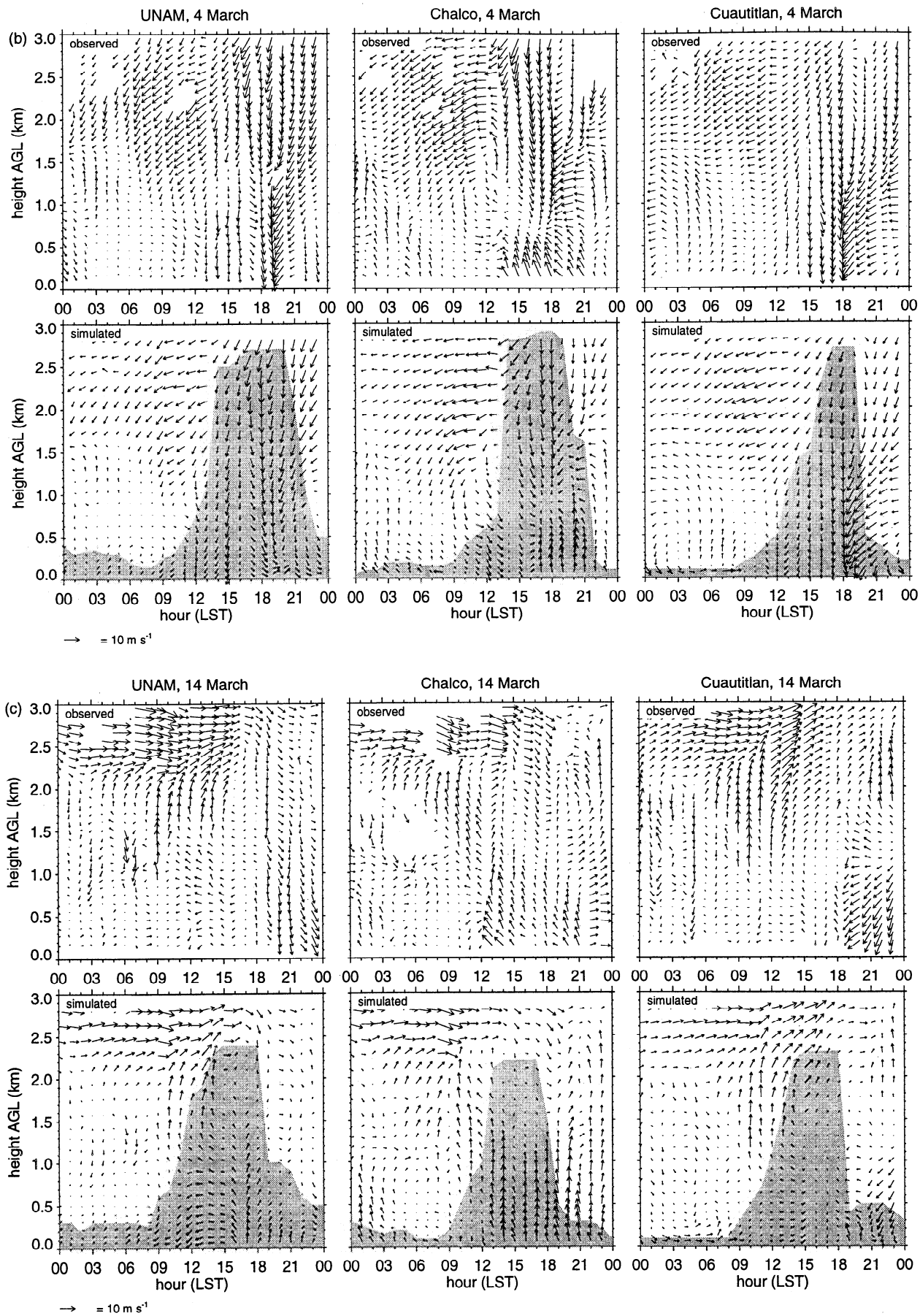

Figure 8. (continued)

observed by the profilers in the late morning and early afternoon between 1 and 2.2 km AGL on March 14.

While the synoptic conditions were significantly different on March 2, 4, and 14, the near-surface winds exhibited three common features. First, the winds within 1 km of the ground were light and variable during the morning hours. The day-to-day variations in the morning wind directions are important for air quality applications, since they probably influence the convergence of ozone precursors within the basin on each day. Even though the winds were light, pollutants can be transported as far as 10 km over a 3-hour period by 1 m s^{-1} wind speeds; however, reactive species may not be transported as far before undergoing chemical transformation. The simulated wind speeds increased during the afternoon as a result of the downward transfer of momentum associated with CBL growth. Second, southerly flow formed over the southeastern gap in the mountains and propagated into the basin through Chalco on each day. In fact, southerly winds were observed at this site in the afternoon on most of the days during the field campaign. The model results indicated that these winds were caused by a north-south temperature and pressure gradient that developed in the afternoon as the basin atmosphere became warmer than the atmosphere over the valley south of Mexico City. The processes responsible for this southerly flow are similar to those associated with a plain-to-basin wind [*de Wekker et al.*, 1998; *Kimura and Kuwagata*, 1993] or a propagating density current [*Bossert and Cotton*, 1994; *Doran and Zhong*, 1994]. Third, strong northerly winds often formed during the field campaign over Cuautitlan and Teotihuacan in the late afternoon and early evening that were due to thermally driven wind systems associated with the elevated heating of the central Mexican plateau. The northerly winds at Cuautitlan and Teotihuacan and the southerly winds at UNAM and Chalco on March 2 and 14 indicate strong convergence within the basin late in the afternoon that may trap pollutants over the MCMA.

4.2. Simulated Horizontal Particle Concentration Fields

The simulated near-surface wind fields and particle concentrations within 100 m of the ground at two times on March 2, 4, and 14 are shown in Figure 9. The observed ozone concentrations and winds from the RAMA network as well as the near-surface winds from the Chalco and UNAM sites are also shown for comparison purposes. The observed wind speeds are smaller than the simulated wind speeds at 26 m AGL (two vector scales are employed) because the instrumentation is located closer to the ground. Since the surface meteorological observations are not assimilated by the model, they are an independent data set that can be used to evaluate the simulated wind fields. The winds from the RAMA network are often not representative of the surrounding conditions because of channeling or distortion of the flow in the urban environment; therefore significant differences between observed and simulated wind direction and speed are expected to occur at times.

Particles were advected to the southwestern side of the basin by near-surface northeasterly winds over the MCMA during most of the morning of March 2. Heating of the basin slopes resulted in northeasterly near-surface winds directed up the south and western basin slopes and westerly near-surface winds up the eastern basin slopes. As Figure 9a shows, the maximum particle concentration at 1400 LST occurred in the vicinity of the highest ozone concentrations at

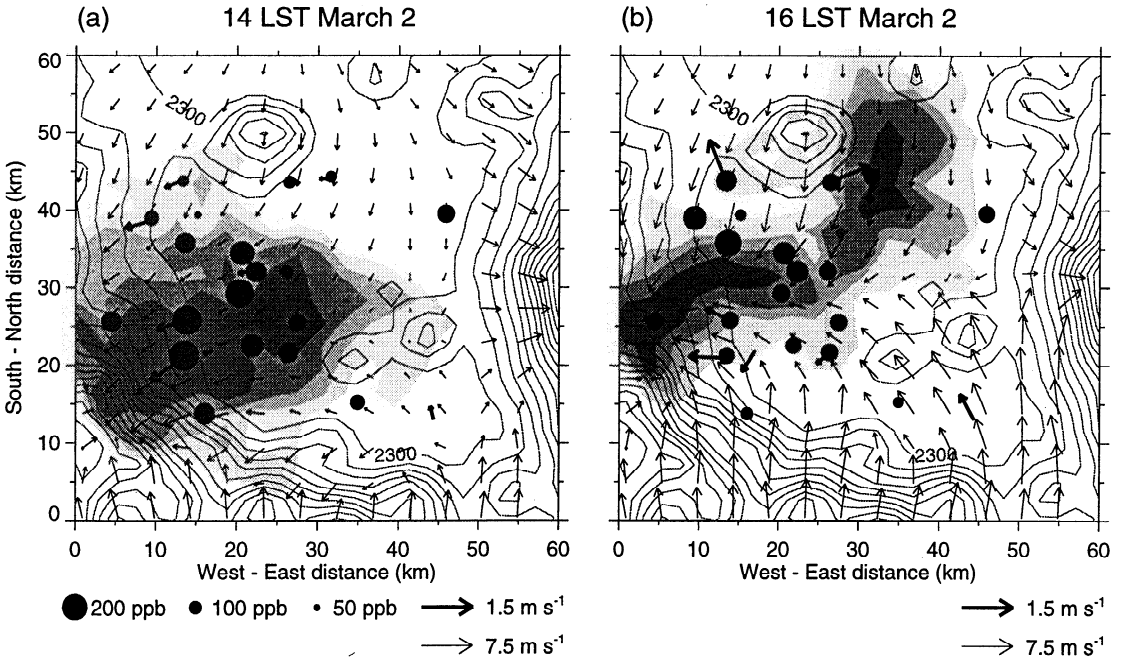

Figure 9. Simulated near-surface horizontal wind vectors and particle concentrations (shaded) over a subsection of the third nested grid at (a) 1400 LST, March 2, (b) 1600 LST, March 2, (c) 1300 LST, March 4, (d) 1700 LST, March 4, (e) 1400 LST, March 14, and (f) 1600 LST, March 14 with topography contours (100-m interval). The size of the solid circles denotes the magnitude of the measured ozone concentration, and the thick vectors denote observed near-surface winds. Particles less than 30 min old are not plotted in order to distinguish the particle plume from fresh emissions.

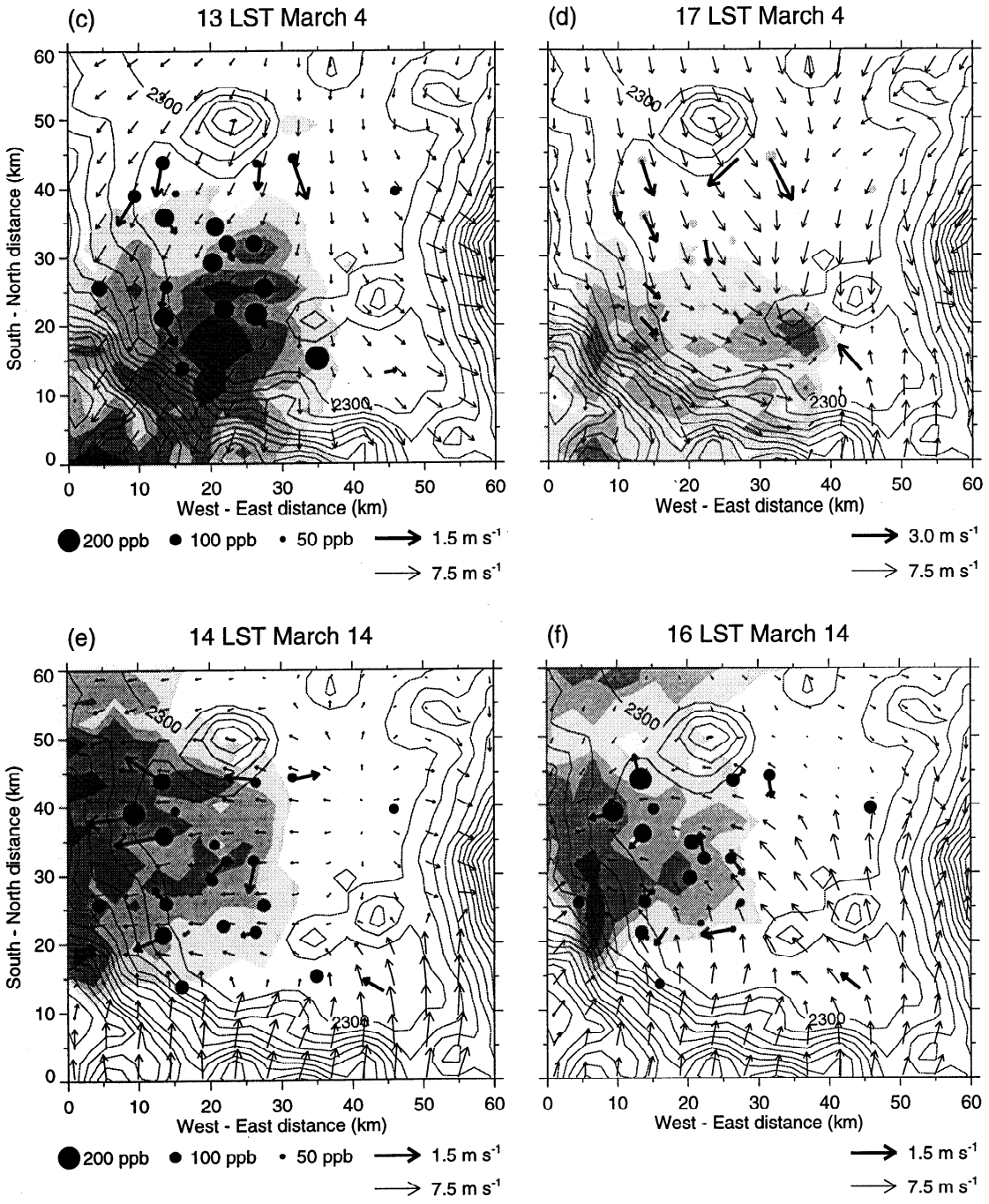

Figure 9. (continued)

the southwest monitoring stations. Southerly flow through the southeastern gap in the mountains and over the southern mountain ridge propagated into the basin after 1400 LST and produced stronger southeasterly winds by 1600 LST over the southern MCMA (Figure 9b), including the UNAM site (Figure 8a). The southerly winds also produced stronger near-surface convergence over the middle of the basin. The maximum particle concentration was advected to the north, consistent with the highest ozone concentrations that occurred at the northwest monitoring stations at this time.

Figure 9c depicts the surface winds and particle concentration field at 1300 LST on March 4. The flow into the basin, the northeasterly winds over the MCMA, and the local slope flows resemble the early afternoon wind field on March 2 (Figure 9a), except that northerly winds are produced over the entire southern basin slopes. The model does not reproduce the anticlockwise circulation exhibited by the observed near-surface winds. Northeasterly upslope flows were produced along the southwestern slopes of basin so that the highest particle concentrations occurred over the southwestern and southeastern MCMA. The highest ozone concentration at this time occurred at Tlahuac (Figure 1), the monitoring station closest to Chalco, but the maximum particle concentrations were located farther to the west. The simulated winds became more westerly over the southern part of the basin later in the afternoon and advected a larger

fraction of particles to the southeast by 1700 LST as shown in Figure 9d. The observed winds were consistent with simulated wind directions the entire afternoon except over the southern basin at 1300 LST. In contrast to March 2, the particle plume was advected by the northerly flow farther to the south beyond the surrounding mountains.

On March 14, particles released during the early morning hours were advected predominately to the southwestern portion of the basin by light surface winds. In contrast to the previous two cases, the surface winds over most of the MCMA became easterly by 1400 LST as shown in Figure 9e. Very light winds were produced over the northeastern portion of the basin, and southerly flow began to develop over the southern basin slopes a few hours sooner than it had on March 2. The highest surface particle concentrations occurred over the northwestern portion of the basin, consistent with the highest ozone concentrations. Particles continued to be advected primarily to the northwest during the rest of the afternoon as the southeasterly flow penetrated into the center of the basin at 1600 LST (Figure 9f).

To further examine the spatial distribution of particles, the fraction of particles within each of the four MCMA sampling domains is shown in Figure 10. On March 2, the largest fraction of particles occurred within the southwest sampling domain, SW_S, during the morning and early afternoon (Figure 10a). Particles were advected primarily into the NW_S and NE_S sampling domains after 1400 LST, decreasing the fraction of particles within sampling domain SW_S. The largest fraction of particles on March 4 occurred in the SW_S and SE_S sampling domains (Figure 10b). Although the southwest portion of the basin usually had the largest fraction most of the afternoon, both of the southern sampling domains had about the same fraction at 1300 and 1600 LST. On March 14 the largest fraction of particles occurred within the NW_S sampling domain during the entire afternoon (Figure 10c).

In general, the highest particle concentrations occurred in the vicinity of the peak ozone concentrations for most of the afternoon for each of the three cases presented in Figures 9 and 10. The spatial patterns of particle concentrations were also consistent with the ozone observations for the February 25 and March 11 simulations. The correspondence between the particle concentrations and the ozone values on March 9 and 18 was not as good as that for the other cases, although there were periods in which the particle distribution resembled the observed spatial ozone patterns. Average ozone concentrations were nearly the same among the five regions on March 9, but the maximum particle concentrations usually occurred over the western portions of the basin. On March 18, maximum particle concentrations were produced in the southwest, rather than in the southeast, where the maximum in the ozone observations occurred.

A statistical analysis of the differences between the observed and simulated winds may explain some of the discrepancies between the locations of the highest particle concentrations and the peak ozone concentrations. For example, the differences between the observed and simulated winds at the UNAM site was somewhat larger on March 11 and 18 than on the other days (not shown). Unfortunately, UNAM wind profiler observations were unavailable on March 9 after 0700 LST, so that the model results cannot be verified during the day. During the afternoon of March 9, northeasterly winds between 4 and 6 m s^{-1} within 0.5 km of the surface simulated over UNAM permitted a large fraction of particles to be advected toward the western portion of the basin. On March 18 the observed winds within the CBL were light and variable between 1300 and 1500 LST, but the simulated easterly and northeasterly winds of 2 to 6 m s^{-1} within 1.5 km of the surface prevented the particle plume from being advected to the southeast. Relatively large near-surface wind field errors over a few hours probably contributed to significant transport errors during both of these cases. These findings demonstrate that FDDA does not always guarantee good agreement between observed and simulated winds, especially when the observed winds are light and variable.

Information from the dispersion model allows the particle source regions to be determined. On March 2, an equal fraction of the particles in the southwest originated from each of the four emission sources. Most of the particles in the southeast on March 4 originated from the two eastern sources, SE_e and NE_e, since the winds were northerly most of the day. Early in the afternoon of March 14 a significant number of particles from each source were found within the northwest sampling domain, but the largest fraction of particles originated from NE_e late in the afternoon. These results demon-

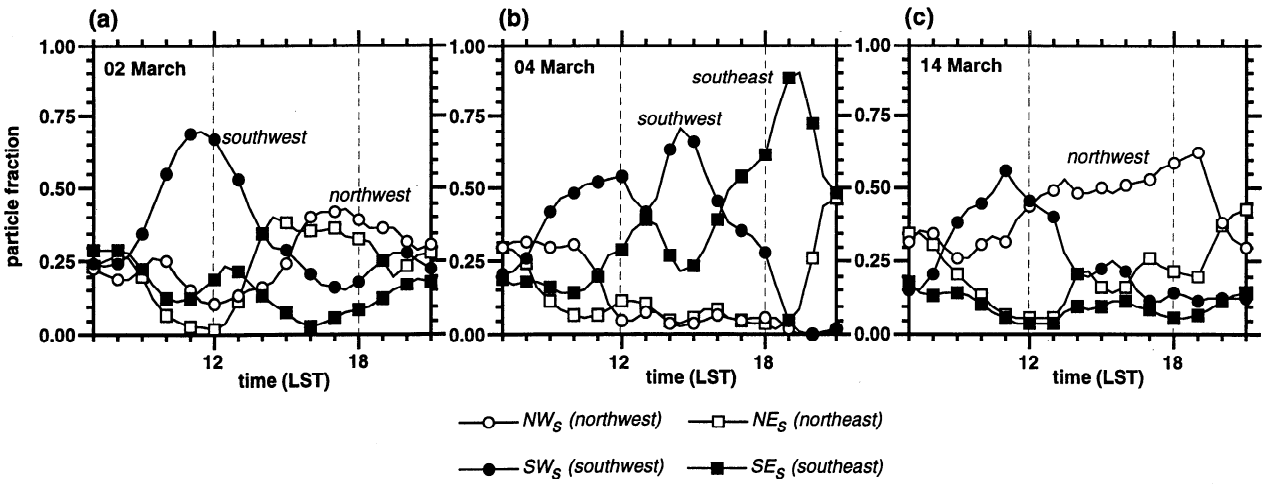

Figure 10. Fraction of particles in each quadrant of the MCMA as defined by sampling domains SW_S, SE_S, NW_S, and NE_S on (a) March 2, (b), March 4, and (c) March 14.

strate that local emissions alone cannot explain the occurrence of high ozone concentrations at specific locations and that different emission sources over the MCMA probably affect specific locations on a daily basis and sometimes on an hourly basis, depending upon the meteorology.

4.3. Simulated Vertical Particle Concentration Fields and Trajectories

Vertical cross sections of the wind, potential temperature, and particle concentrations (Figures 11, 13, and 15) and representative kinematic forward trajectories of particles (Figures 12, 14, and 16) are used to illustrate the atmospheric mechanisms aloft associated with the surface concentrations presented in the previous section.

Light, near-surface winds advected particles that were released early in the morning on March 2 toward the southwest (not shown). Upslope flows subsequently advected the particle plume up the western and southern basin slopes within a shallow CBL by 1100 LST. Particles over the slopes between 1100 and 1200 LST were mixed upward by vertical diffusion processes and vented out of the CBL into the free atmosphere, a process also known as "mountain venting" or the "mountain-chimney effect" [*Lu and Turco*, 1994]. Strong vertical wind shears were simulated by the model so that southwesterly winds advected the layer of particles vented out of the CBL back over the city by 1300 LST, as shown in Figure 11a. Particles within this layer were entrained into the CBL when the mixed layer over the city grew to a height of 1.2 km AGL. Mean sinking motions associated with the return flow were also responsible for bringing particles down

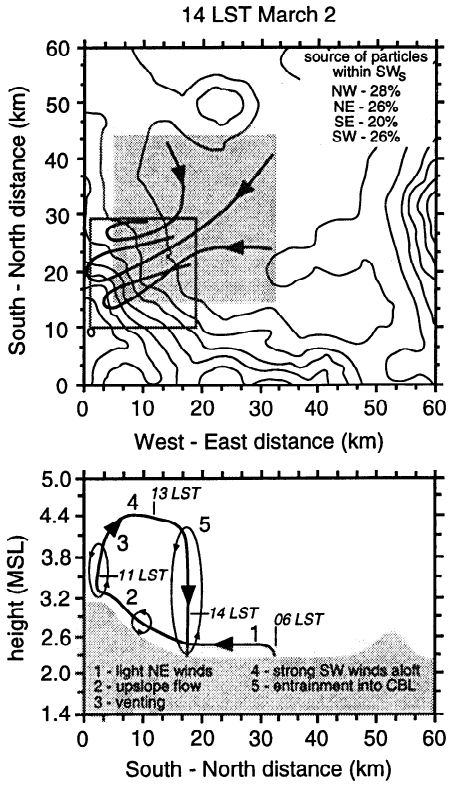

Figure 12. Horizontal and vertical cross sections depicting representative trajectories ending at 1400 LST on March 2, where the gray area denotes the four sources employed by the particle model, the boxes denote the sampling domains, and the ellipses represent mixing within the convective boundary layer.

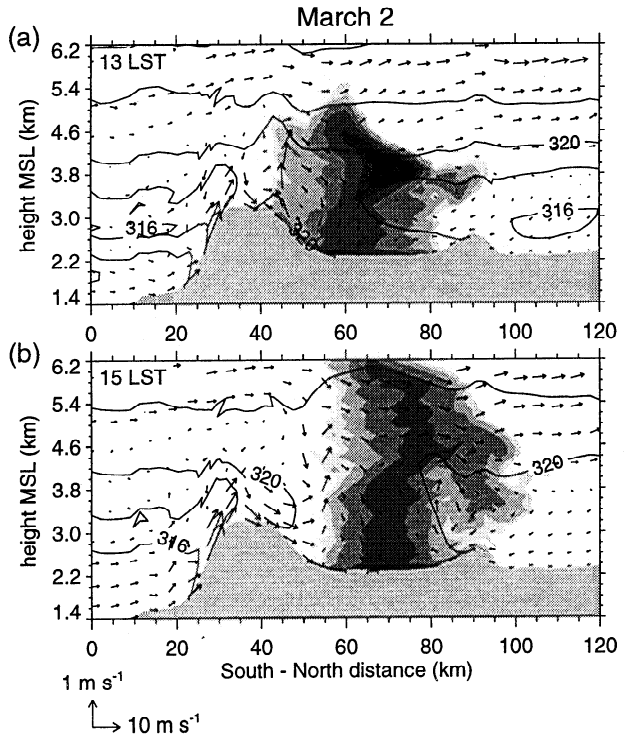

Figure 11. North-south vertical cross section of particle concentration (shaded), potential temperature (contours), and wind (v and w component wind vectors) at (a) 1300 LST, March 2, and (b) 1500 LST, March 2. Vertical cross section located near x=20 km on Figure 9.

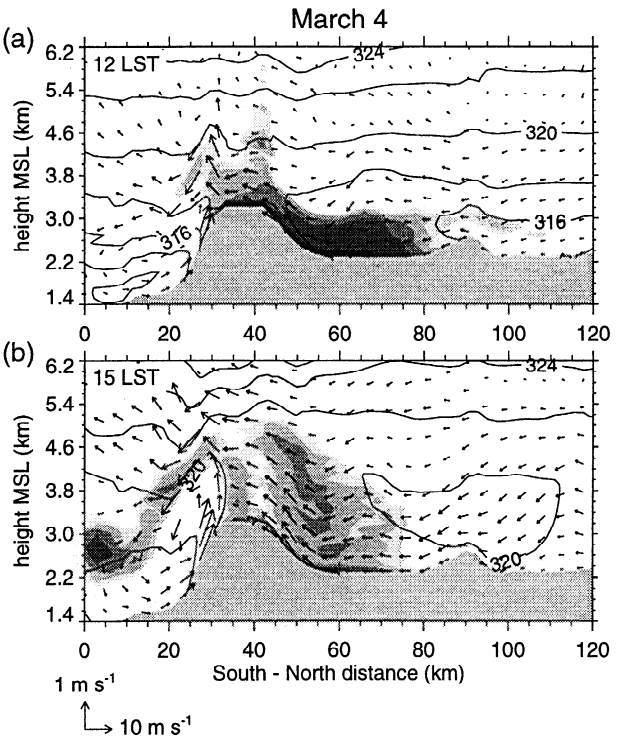

Figure 13. Same as Figure 11 except at (a) 1200 LST, March 4 and (b) 1500 LST, March 4.

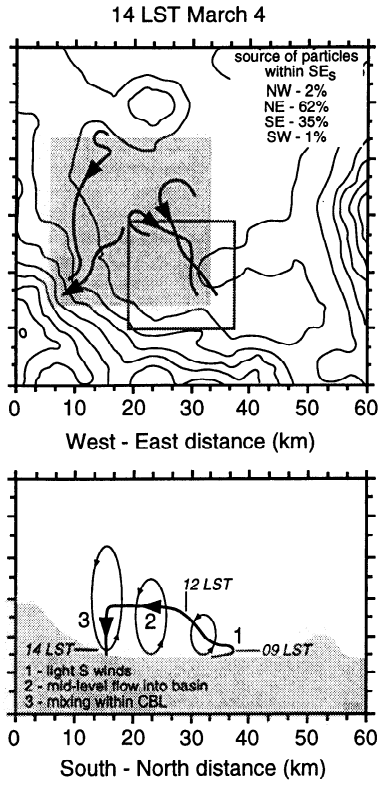

Figure 14. Same as Figure 12 except on March 4.

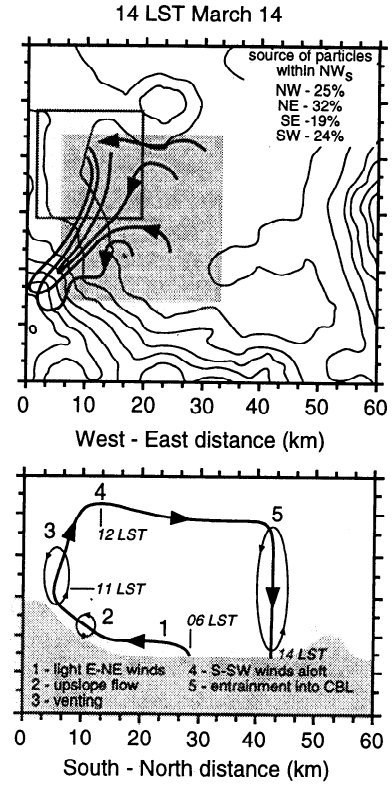

Figure 16. Same as Figure 12 except on March 14.

to the surface. Trajectories of particles emitted early in the morning from all four area sources (Figure 12) exhibited recirculation patterns associated with the mountain venting and entrainment processes. High particle concentrations over the southwestern basin were due to both near-surface horizontal advection and entrainment of particles from aloft, indicating that many emission sources may have contributed to the high ozone concentrations in this region. The entire particle plume was advected to the north by 1500 LST as the simulated density current developed over the southern ridge (Figure 11b) and as the westerly winds aloft decreased in intensity and became southerly (Figure 8a). Near-surface convergence in the middle of the basin produced strong upward vertical motions that transported particles toward the top of the CBL, where horizontal winds between 5 and 10 m s^{-1} quickly advected the particle plume out of the basin atmosphere. This process, defined here as "basin venting" and called the "stovepipe effect" by *Jauregui* [1988], efficiently reduced surface particle concentrations after 1500 LST.

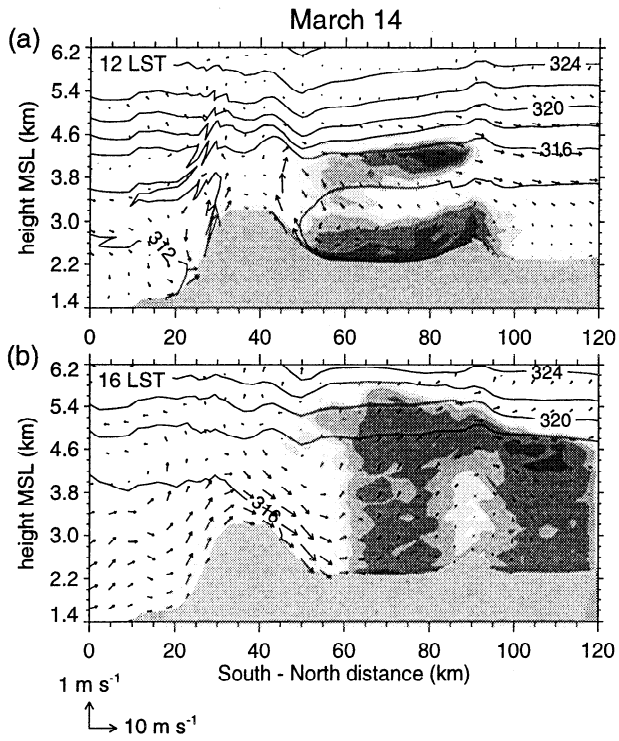

Figure 15. Same as Figure 11 except at (a) 1200 LST, March 14, and (b) 1600 LST, March 14.

On March 4, upslope flows along the southern basin slopes were coupled to the upper-level northerly winds so that relatively small wind direction shears were produced as shown in Figure 13a. Particles were confined to within 0.6 km of the ground until noon as they were advected from the MCMA over the mountain ridge. As the CBL grew during the afternoon, particles were mixed up to 1.5 km AGL by 1500 LST as shown in Figure 13b. Particles vented out of the CBL into the free atmosphere over the mountains were advected toward the south, in contrast to the events of March 2. As shown by the trajectories in Figure 14, particles emitted from eastern sources after 0900 LST were mixed throughout the growing CBL as they were advected by the northerly flow to the southeastern end of the basin. Only a small fraction of the particles emitted from the western sources was advected to the eastern side of the basin. Trajectories did not exhibit recirculation patterns like those on March 2, since there were no substantial wind direction shears.

The atmospheric processes on March 14 were similar to those on March 2 in many respects; however, subtle differences in the wind shears affected the placement of the maximum number of particles. For example, particles were vented out of the CBL on this day into the layer of moderate southerly winds observed by the profilers (Figure 8c). The 5 m s^{-1} winds aloft advected the layer of particles to the northern portion of the basin by 1200 LST as shown in Figure 15a. As the CBL grew, this layer was entrained into the CBL as the entire particle plume over the MCMA was advected to the north (Figure 15b). The particle trajectories shown in Figure 16 are similar to those on March 2, except for the longer transport distance aloft. While the midlevel winds over the basin slopes were southwesterly, the particle plume was turned to the north by more southerly winds over the MCMA. The persistent high particle concentrations over the northwestern end of the basin were due to both entrainment and near-surface convergence. The different CBL growth rates and the wind directions and speeds aloft on March 2 and 14 resulted in variations in the recirculation patterns and entrainment locations.

To further demonstrate the importance of pollutant recirculation, the age distribution of particles over individual sampling domains on March 2, 4 , and 14 is shown in Figure 17. About 30% of the particles within SW_S on March 2 (Figure 17a) were between 4 and 8 hours old at 1400 LST, the time of the maximum ozone concentration; therefore recirculation (Figure 12) may have been an important mechanism contributing to the high ozone concentrations. The shorter times of the remaining 70% of the particles were associated with the horizontal advection of particles recently released, because there were no other sources upwind of Mexico City, and moderate wind speeds advected older particles beyond the MCMA sampling domains in 4 hours. On March 4 (Figure 17b), nearly 75% of the particles within SE_S were less than 2 hours old at 1300 LST because the higher near-surface wind speeds reduced the transport time of particles advected into and out of the sampling domain. Only a very small fraction of the particles were greater than 4 hours old the entire day, demonstrating that the particle plume was not recirculated over the MCMA. The high ozone concentrations in the southeast cannot be explained by the newly emitted particles, since photochemistry takes at least 3 to 4 hours to produce high concentrations of ozone from primary emissions of NO_x and reactive hydrocarbons in a typical urban atmosphere. This finding implies that the anticlockwise near-surface circulation (Figure 9c) may be much stronger than the simulated one, so that the basin atmosphere was less well ventilated. A relatively large fraction of the particles on March 14 (Figure 17c) within NW_S were 4 to 8 hours old between 1200 and 1500 LST, somewhat earlier than the peak ozone concentrations that occurred between 1400 and 1800 LST. The model results suggest that recirculation may have been an important factor early in the afternoon but relatively unimportant in the late afternoon. In fact, the near-surface wind directions became easterly late in the afternoon, so that most of the particles were advected directly from NE_e in less than 2 hours.

The recirculation on March 2 and 14 suggests that pollutants would remain trapped within the basin atmosphere during the day; however, the strong winds on March 4 indicate that the basin atmosphere can also be well ventilated. To quantify the ventilation of the basin atmosphere, the particle loss with time within the four MCMA sampling domains was computed for all seven cases, with results shown in Figure 18. A value of 1 means that all particles emitted up to that time on that day remain over the MCMA. Values greater than 1 occur when particles emitted on the previous day remained over the MCMA. In general, particles emitted during the morning were advected by light winds and trapped within a shallow boundary layer over the MCMA. During the afternoon as the boundary-layer depth grew substantially between 1100 and 1300 LST, the basin atmosphere became well ventilated. As we expected, the strong northerly winds on March 4 advected a large fraction of the particles out of the basin, so that only 20% remained by 1400 LST. Because of the lighter winds and recirculation patterns, 90% of particles remained over the MCMA at 1400 LST on March 2. The results from the other cases fell between the March 2 and 4 cases, with the fraction of particles remaining over the MCMA gradually dropping off during the afternoon. The southerly winds at Chalco and northerly winds at Cuautitlan and Teotihuacan imply that convergence would trap pollutants within the basin atmosphere; however, vertical diffusion and mean vertical motions due to the near-surface convergence transported particles upward where stronger winds aloft usually advected a large fraction of the particle plume out of the basin atmosphere.

Clearly, a three-dimensional interpretation of the meteorology is needed to understand the ventilation of pollutants in

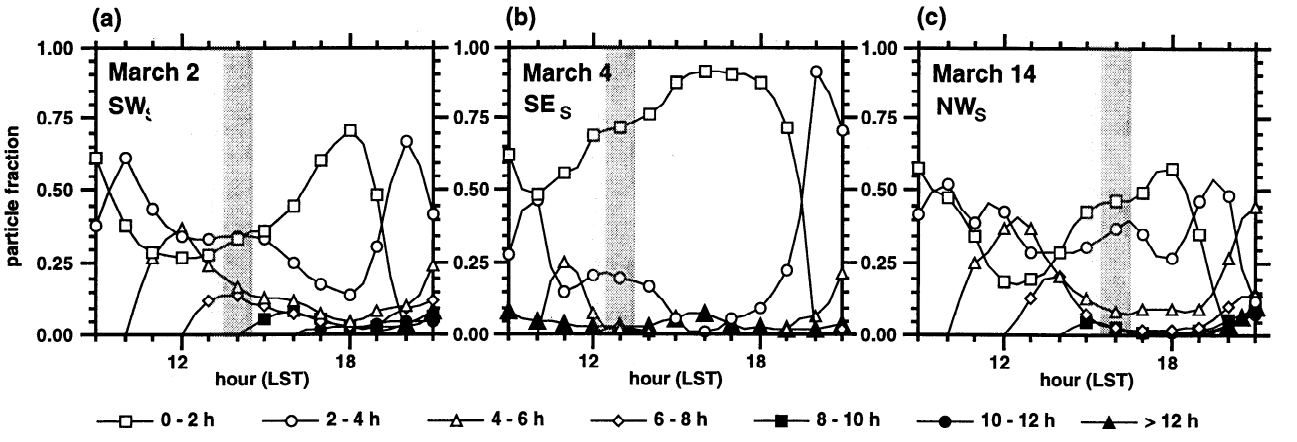

Figure 17. Age of particles within sampling domain (a) SW_S on March 2, (b) NE_S on March 4, and (c) NW_S on March 14, where the vertical gray lines denote the time of the observed maximum ozone concentration.

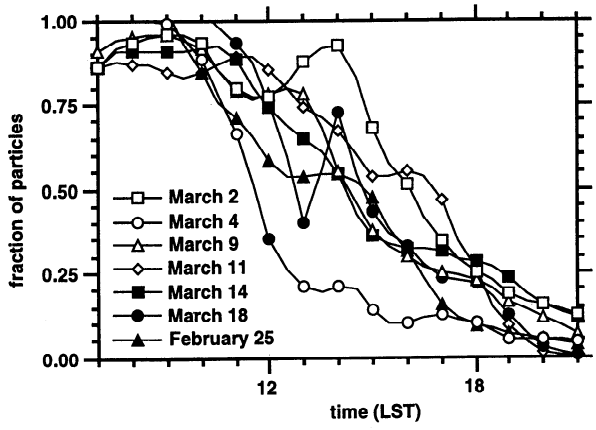

Figure 18. Fraction of particles remaining over the MCMA (SW_S, SE_S, NW_S, and NE_S sampling domains) for all seven cases between 0900 and 2100 LST.

the vicinity of Mexico City. The measurements made during the field campaign are insufficient, by themselves, to describe all of the atmospheric processes responsible for pollutant dispersion.

4.4. Previous Day Emissions

The fraction of particles in Figure 18 exceeded 1 early in the morning for some of the cases because some of the particles emitted the previous afternoon remained within the basin atmosphere or were transported back over the basin by 0600 LST. Since the winds were often light and variable at night, pollutants emitted on one day may have an impact on air chemistry the following day. It has not been possible until now to estimate the potential impact of previous day emissions, since the spatial variation of the winds aloft in the vicinity of Mexico City had not been measured prior to the 1997 IMADA-AVER field campaign. The three-dimensional meteorological fields produced by the observations and the mesoscale model with FDDA provide the information needed to estimate residence time of air parcels in the basin atmosphere at night.

The fraction of particles remaining within the basin atmosphere, as defined by sampling domain B_S, during the first evening, is shown in Figure 19a. At the end of the afternoon (1800 LST) the fraction of particles within B_S was between 30% and 50% of the total particles emitted during the day for five of the cases and less than 15% for the other two cases. Even though the measured winds were usually light (Figure 8), the fraction of particles gradually decreased during the evening as more and more particles were advected out of the basin. This finding is not surprising because a 1 m s^{-1} wind would advect a particle over 43 km downwind (approximately basin width) during a 12-hour nocturnal period assuming a constant wind direction. By 0600 LST of the second day the particle fraction that remained over B_S was less than 13% of the total particles emitted the previous day in all cases. Layers of particles at 0600 LST were distributed at different elevations within 2 km AGL for each case (Figure 19b).

An analysis of the average observed wind speeds during the evening did not indicate a strong correlation between low wind speeds and relatively high particle concentration layers at 0600 LST. Even though the winds were weak, wind direc-

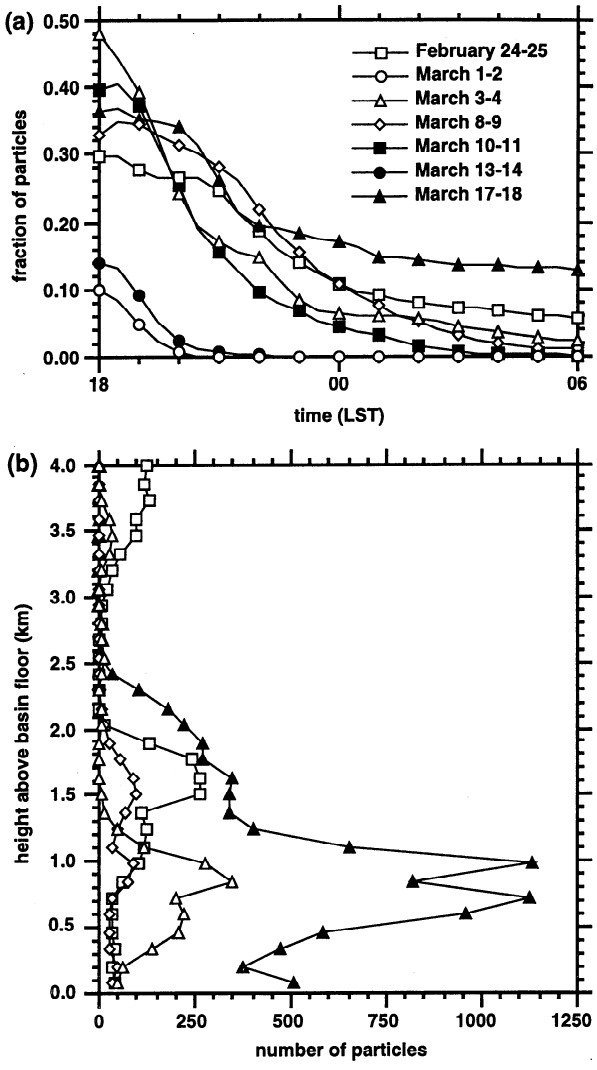

Figure 19. (a) Fraction of particles within the basin atmosphere as defined by the B_S sampling domain during the first evening between 1800 and 0600 LST for all seven cases and (b) instantaneous vertical particle profile from the B_S sampling domain at 0600 LST.

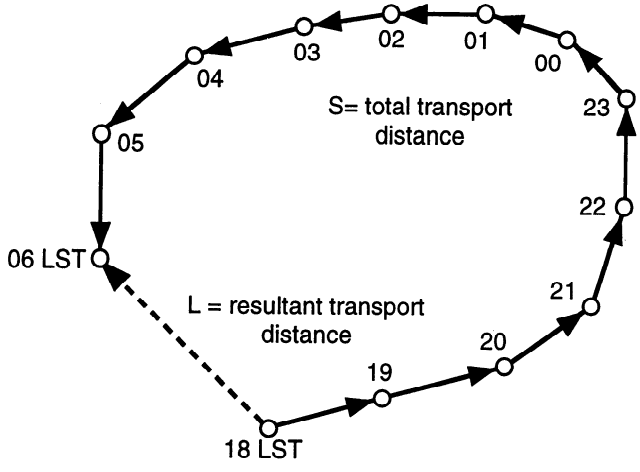

Figure 20. Illustration of the definition of total transport distance, S, and resultant transport distance, L, used to define the recirculation parameter, R, for a single particle trajectory.

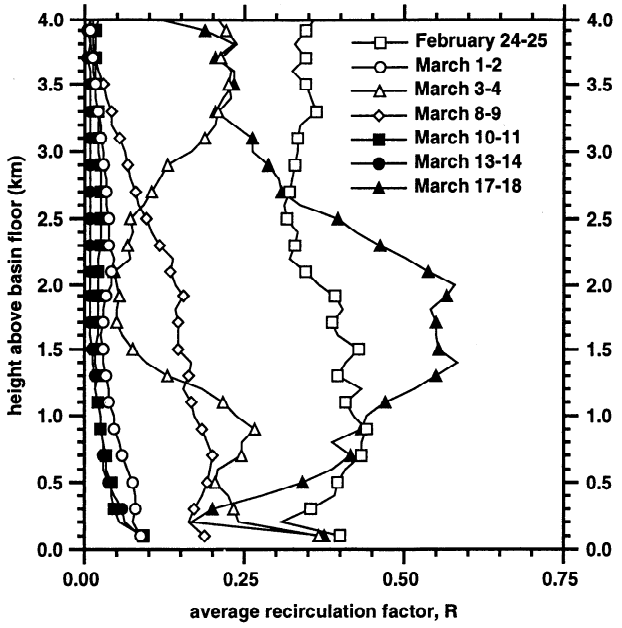

Figure 21. Vertical profile of the average recirculation factor, R, for all seven cases, assuming 12-hour trajectories starting at 1800 LST on the first afternoon.

tion variation was also important in determining whether an air parcel remained within the basin over a 12-hour period. A recirculation parameter, R, based on air parcel trajectory characteristics was therefore calculated to account for wind direction variations [*Allwine and Whiteman*, 1994]. In this study, R is defined as

$$R_i = 1 - \frac{L_i}{S_i} \qquad (0 \le R \le 1) \qquad (1)$$

where i denotes the trajectory number, S is the length of the trajectory, and L is the resultant transport distance over a 12-hour time period as shown in Figure 20. When R is equal to 0, straight-line transport has occurred. When R is equal to 1, no net transport has occurred over the 12-hour time period, and there has been complete recirculation. Additional particle model simulations were performed for each case in which 10^5 particles were randomly distributed within 3 km of the surface over the MCMA at 1800 LST on the first day. R was calculated for each 12-hour particle trajectory. An average value of R at 0600 LST as a function of initial elevation is shown in Figure 21.

The evening of March 17-18 produced the largest values of R, corresponding to the highest fraction of particles remaining within the basin (Figure 21). February 25 produced the next highest values, followed by March 4 and 9, also corresponding to the fraction of particles shown in Figure 19b. R varied significantly, depending upon the initial horizontal position and elevation of the trajectory. There were many trajectories with values of R of about 0.95 and transport distances under 10 km during the evening of March 17-18, but particles initially located over the eastern MCMA were advected out of the basin atmosphere, resulting in an average value of R of about 0.5. A common feature among the cases was that a substantially higher fraction of particles initially located over the western or southwestern end of the basin at 1800 LST remained within the basin atmosphere than did particles initially located over the eastern end of the basin. These findings are consistent with the aircraft data analyses from the 1991 MARI field campaign that identified the central and southwest portions of the MCMA to have the highest levels of pollutants aloft in the morning [*Díaz-Francés et al.*, 1994].

While the total particle fraction was small on the morning of March 18, it was equivalent to about an hour's worth of emissions. Entrainment of pollutants from the layer aloft (Figure 19b) into the growing CBL would contribute to surface concentrations by the early afternoon, but the pollutants would be distributed throughout a deep mixed layer so that the impact on surface concentrations might be small unless the concentrations aloft were sufficiently high. While meteorological conditions may exist that can trap a significant fraction of pollutants within the basin atmosphere, the results from the seven cases examined in this study suggest that emissions from the previous day are a minor contribution to air chemistry on the following day. It is possible that vehicular and industrial emissions trapped in the surface-based inversion layer at night (between 1800 and 0600 LST) contribute to high near-surface pollutant concentrations in the morning, but our interest here is the contribution of pollutants from the residual layer aloft by entrainment.

5. Discussion

The correspondence between the calculated particle concentration fields and the observed spatial ozone patterns suggests that the mesoscale analyses based on the model and the observed profiles of wind and temperature from the field campaign captured the main flow features responsible for the inhomogeneous ozone concentrations within the basin, including the winds over the basin slopes and floor. The highest particle concentrations usually occurred in the vicinity of the peak ozone concentrations during the afternoon. The observations, mesoscale analyses, and particle distributions provided evidence that the circulations in the vicinity of the MCMA are highly complex.

In addition to near-surface convergence, three-dimensional recirculation was also found to contribute to the spatial variations in the particle concentration fields. In general, the spatial inhomogeneities in the wind fields redistributed the particles within the basin in the morning hours and subsequently affected the maximum particle concentration in the afternoon. Particles were advected by local slope flows over the mountainous areas to the west and south of the city during the day. A large fraction of these particles were vented out of the CBL into the free atmosphere (mountain venting), producing an elevated layer of particles aloft. When vertical wind shears were present, the elevated particle layer was advected back over the MCMA (recirculation) and mixed down to the surface by vertical diffusion processes associated with the growth of deep CBLs. The mixed layer depth and the midlevel wind directions and speeds determined when and where particles were entrained into the growing CBL, implying that an accurate treatment of this interaction is necessary in reproducing the spatial ozone distributions by air quality models.

The contribution of emissions from the previous day was found to be relatively minor for the seven periods examined in this study, suggesting that the high ozone concentrations are not due to multiday accumulation of pollutants. Particles located over the southwestern portions of the MCMA at

sunset were more likely to remain within the basin than were particles released from other locations within the basin. On the other hand, morning emissions were trapped near the surface within shallow boundary layers over the MCMA. The basin atmosphere became increasingly ventilated during the afternoon as deep mixed layers developed; however, recirculation of particles reduced the rate of ventilation on some days. Southerly winds through the southeastern gap in the mountains and northerly winds at the north end of the basin produced convergence and strong upward vertical motions in the model over the center of the basin late in the afternoon. The mean vertical velocities coupled to mixing processes in the CBL transported particles up to several kilometers AGL, where stronger winds advected the particle plume downwind of Mexico City (basin venting). The near-surface convergence patterns varied from day to day, depending upon the timing and strength of the regional northerly and southerly thermally driven wind systems. These results demonstrate that air quality models should adequately represent the complex convergence patterns and magnitude of the vertical velocities when predicting the reduction of ozone and other pollutants within the basin during the late afternoon.

Despite the encouraging results, some caution should be applied in using the mesoscale analyses to determine the meteorological factors associated with pollutant transport over Mexico City. For example, even though there was good agreement between the simulated near-surface wind directions and the RAMA wind directions, it is not clear how well the RAMA stations represent the winds just above the height of the buildings and trees. On the basis of the observations at UNAM and Chalco the model probably overpredicted the strength and depth of the near-surface daytime upslope and nighttime downslope winds at times. There were no wind observations over the mountainous areas surrounding the MCMA to verify whether the model predicted the slope winds correctly. An additional wind profiler located in the vicinity of the airport would have been useful in obtaining wind field characteristics over the center of the MCMA and determining how far the southerly and northerly thermally driven circulations penetrated into the basin. Uncertainties associated with the winds in these regions affect the findings regarding the transport and recirculation of particles within the basin. Overprediction of the nighttime drainage winds may have been partially responsible for the simulated near-surface temperatures that were too cool early in the morning. These low temperatures also may have been due to uncertainties associated with the surface energy budget, such as the specification of a dry, constant initial soil moisture value. Showers occurred in the Mexico City area, producing inhomogeneous soil moisture distributions during the latter part of the field campaign. Another process not accounted for by the mesoscale model is the urban heat island effect. It is possible that omission of this process may explain why the simulated surface temperatures are too low in the morning. Surface temperatures over Mexico City have been observed to be 4° to 5°C warmer than those over the surrounding areas at night [*Jauregui*, 1988, 1997], but the impact of the urban heat island on local circulations has been difficult to assess because of the uncertainties associated with the surface wind measurements in the city.

Even though there are still some uncertainties associated with the meteorological conditions, the particle model results indicate that a chemistry model employing the mesoscale analyses will probably capture the overall spatial and temporal behavior of ozone in the basin, if emissions are known. A chemistry model applied for these days may predict the correct ozone concentration, but the Eulerian framework of many chemistry models would make it difficult to determine how the various meteorological processes affected ozone transport. The particle model approach proved to be useful in identifying several atmospheric processes responsible for pollutant transport within the basin, including horizontal advection, recirculation, mean vertical motions, vertical diffusion, mountain venting, and basin venting. The complexity of the meteorology will also affect box model studies that evaluate the relative importance of various chemical reactions. Simple box model formulations cannot represent three-dimensional circulations that advect emissions from one region to another; therefore comparisons of their results with air chemistry observations over Mexico City may be misleading.

Since simulating the transport of reactive chemicals, such as ozone, with the use of a passive tracer has obvious limitations, the mesoscale model analyses presented in this study will be used in the near future as input to a photochemical model to examine the effect of variable emissions and air chemistry mechanisms on spatial ozone patterns within the Mexico City Basin. Emission inventories for Mexico City are currently being developed by other IMADA-AVER participants.

6. Summary

Meteorological and air chemistry observations made during the 1997 IMADA-AVER field campaign, a mesoscale model, and a particle dispersion model have been employed to identify the atmospheric mechanisms associated with spatial ozone patterns over the MCMA. During this field campaign, detailed measurements of the spatial structure of flows within the basin was obtained for the first time. Meteorological observations were incorporated into the mesoscale model by using four-dimensional data assimilation to produce analyses, with high temporal and spatial resolution, that describe the boundary-layer development and circulations in the vicinity of Mexico City. A Lagrangian particle dispersion model employed these analyses to help identify the meteorological factors associated with the observed inhomogeneous ozone concentrations within the basin.

As we expected, the mesoscale model analyses reproduced many features of the observed temperature and wind profiles within the basin. The mesoscale analyses and the observations demonstrated that the boundary layer often exhibited a strong diurnal variation with a strong surface-based inversion at night and a deep mixed layer during the afternoon because of the high elevation, low latitude, and dry winter conditions. Circulation patterns in the lower atmosphere were complex as a result of local- and regional-scale thermally driven flows and their interaction with the upper-level synoptic winds. The correspondence between the calculated particle concentration fields and the observed spatial ozone patterns suggests that the mesoscale analyses captured the main flow features responsible for the inhomogeneous ozone concentrations within the basin, including the winds over the basin slopes and over the basin floor where no measurements were made. The complex circulations had a significant impact on the day-

to-day variations in the spatial particle distributions in the basin, implying that transport plays a role just as important as that of local ozone production in determining the spatial ozone distributions over the MCMA.

Several meteorological processes responsible for pollutant transport within the basin were identified, including horizontal advection, near-surface convergence, recirculation, mean vertical motions, vertical diffusion, mountain venting, and basin venting. Since high ozone concentrations occur almost every day over the MCMA, one might expect that the surrounding mountains act to trap pollutants from one day to the next. However, the particle model results indicate that contributions from previous day emissions are probably small. Instead it is more likely that emissions trapped within the surface-based inversion during the evening and early morning ultimately contribute to the high ozone values observed during the afternoon.

The particle model results demonstrate that ozone over Mexico City may be very sensitive to flow phenomena. As *Fast* [1998] showed, mesoscale model forecasts in basin topographies may produce relatively large errors, especially when winds are light, that will contribute to uncertainties in ozone transport predicted by chemistry models. Data assimilation can be used to reduce the uncertainties associated with the meteorology, but additional simulations without FDDA for periods of the 1997 field campaign are necessary to further evaluate the boundary-layer characteristics predicted by the mesoscale model. This is an important task, since mesoscale model forecast errors associated with highly complex terrain need to be reduced for more routine air quality model applications for Mexico City and other megacities located in complex terrain.

Appendix

A nudging FDDA technique has been incorporated into the mesoscale model [*Fast*, 1995]. This technique adds a tendency term of the form $-Gw_{xy\sigma}w_t(V_o - V_m)$ to the governing equations, where G is the nudging coefficient, $w_{xy\sigma}$ is the spatial weighting function, w_t is the temporal weighting function, V_o is the observed variable analyzed at a given grid point, and V_m is the model variable at a given grid point. For our application, G is set to 8.3×10^{-4} s^{-1}, and the spatial weight for the third nested grid becomes zero 15 km from an observation site near the surface. This distance increases with height to 20 km at about 5 km AGL. With the exponential covariance model the spatial weight decreases by at least a factor of e^{-1} at a horizontal distance of 10 km from the observation location. Because the spatial weight becomes zero in data sparse regions, only the model governing equations are used to predict the meteorological quantities outside the basin (Figure 6b). The distances associated with the spatial weights become larger on grids 1 and 2, so that the rawinsonde observations (Figure 6a) influence a larger area of the model results. The temporal weight becomes zero 40 min before and after the time of a particular observation; therefore only the model physics are used between the times of the five radiosondes to predict the temperature and humidity evolution within the basin. Relatively large differences between the near-surface model results and the observations occurred sometimes (i.e., for the Chalco site on March 4 shown in Figure 8b) because the FDDA tendencies were small in relation to the other physical terms near the ground. Without FDDA the mesoscale model qualitatively predicts the features observed by the wind profilers and radiosondes; however, significantly larger wind field errors can be produced at times, as *Fast* [1998] described.

Acknowledgments. This research was supported by the U.S. Department of Energy (DOE) as part of the Atmospheric Studies in Complex Terrain (ASCOT) program of the Office of Biological and Environmental Research (OBER). Meteorological data from the field campaign were provided by scientists at DOE's Argonne National Laboratory, Los Alamos National Laboratory, Pacific Northwest National Laboratory, and NOAA's Environmental Technology Laboratory. We would like to thank W. R. Barchet, C. M. Berkowitz, S. F. J. de Wekker, J. C. Doran, J. M. Hubbe, W. J. Shaw, and C. D. Whiteman for their valuable comments on this paper. Pacific Northwest National Laboratory is operated for the U.S. Department of Energy by Battelle Memorial Institute under contract DE-AC06-76RL0 1830.

References

Allwine, K. J., and C. D. Whiteman, Single-station integral measures of atmospheric stagnation, recirculation, and ventilation, *Atmos. Environ., 28,* 713-721, 1994.

Berkowitz, C. M., J. D. Fast, S. R. Springston, R. J. Larsen, C. W. Spicer, P. V. Doskey, J. M. Hubbe, and R. Plastridge, Formation mechanisms and chemical characteristics of elevated photochemical layers over the northeast United States, *J. Geophys. Res., 103,* 10,631-10,647, 1998.

Bian, X., C. W. Whiteman, G. S. Iglesias, and E. W. Garcia, Climatological analyses of air pollution in the Mexico City basin, paper presented at 10th Joint Conference on the Applications of Air Pollution Meteorology with the Air and Waste Manage. Assoc., Am. Meteorol. Soc., Phoenix, Ariz., Jan. 11-16, 1998.

Bossert, J. E., An investigation of flow regimes affecting the Mexico City region, *J. Appl. Meteorol., 36,* 119-140, 1997.

Bossert, J. E., and W. R. Cotton, Regional-scale flows in mountainous terrain, II, Simplified numerical experiments, *Mon. Weather Rev., 122,* 1449-1471, 1994.

Bravo, J. L., M. T. Diaz, C. Gay, and J. Fajardo, A short term prediction model for surface ozone at southwest part of Mexico valley, *Atmósfera, 9,* 33-45, 1996.

Chen, S., and W. R. Cotton, A one-dimensional simulation of stratocumulus-capped mixed layer, *Boundary Layer Meteorol., 25,* 289-321, 1983.

Collins, C. O., and S. L. Scott, Air pollution in the valley of Mexico, *Geogr. Rev., 2,* 119-133, 1993.

Davies, H. C., A lateral boundary formulation for multi-level prediction models, *Qt. J. R. Meteorol. Soc., 102,* 405-418, 1976.

de Wekker, S. F. J., S. Zhong, J. D. Fast, and C. D. Whiteman, A numerical investigation of the plain-to-basin wind. *J. Appl. Meteorol., 37,* 606-622, 1998.

Díaz-Francés, E., M. E. Ruíz, and G. Sosa, Spatial stratification and multivariate analyses of Mexico City air pollution data, paper presented at Second International Conference on Air Pollution, Computational Mechanics Publ., Barcelona, Spain, Sept. 27-28, 1994.

Doran, J. C., and S. Zhong, Regional drainage flows in the Pacific Northwest, *Mon. Weather Rev., 122,* 1158-1167, 1994.

Doran, J. C., S. Zhong, and C. M. Berkowitz, Meteorological factors affecting ozone profiles over the western North Atlantic, *J. Geophys. Res., 101,* 28,701-28,710, 1996.

Doran, J. C., et al., The IMADA-AVER boundary-layer experiment in the Mexico City area, *Bull. Am. Meteorol. Soc.*, in press, 1998.

Fast, J. D., Mesoscale modeling in areas of highly complex terrain, *J. Appl. Meteorol., 34,* 2762-2782, 1995.

Fast, J. D., Observational requirements for describing circulations within the Mexico City basin using four-dimensional data assimilation, paper presented at 10th Joint Conference on the Applications of Air Pollution Meteorology with Air and Waste Manage. Assoc., Am. Meteorol. Soc., Phoenix, Ariz., Jan. 11-16, 1998.

Fast, J. D., and C. M. Berkowitz, A modeling study of boundary layer processes associated with ozone layers observed during the 1993 North Atlantic Regional Experiment, *J. Geophys. Res., 101,* 28,683-28,699, 1996.

Fast, J. D., S. Zhong, and J. C. Doran, Boundary layer processes within the Mexico City basin and their impact on spatial ozone patterns, 2, Dispersion simulations, paper presented at 12th Symposium on Boundary Layers and Turbulence, Am. Meteorol. Soc., Vancouver, B. C., Canada, July 28 to Aug. 1, 1997.

Fuentes-Gea, V., and A. Garcia-Gutierrez, Air pollution trends in Mexico City, TSP (1976-1984), paper presented at 83rd Annual Meeting of the Air and Waste Management Association, Pittsburgh, Pa., June 24-29, 1990.

Garfias, J., and R. González, Air quality in Mexico City, *in The Science of Global Change: The Impact of Human Activities on the Environment*, pp. 149-161, Am. Chem. Soc., Washington, D. C., 1992.

Harms, D. E., S. Raman, and R. V. Madala, An examination of four-dimensional data-assimilation techniques for numerical weather prediction, *Bull. Am. Meteorol. Soc., 73,* 425-440, 1992.

Helfand, H. M., and J. C. Labraga, Design of a nonsingular level 2.5 second-order closure model for the prediction of atmospheric turbulence, *J. Atmos. Sci., 45,* 113-132, 1988.

Hurley, P., and W. Physick, A Lagrangian particle model of fumigation by breakdown of the nocturnal inversion, *Atmos. Environ., Part A, 25,* 1313-1325, 1991.

Jauregui, E., Local wind and air pollution interaction in the Mexico basin, *Atmósfera, 1,* 131-140, 1988.

Jauregui, E., Heat island development in Mexico City, *Atmos. Environ., 31,* 3821-3831, 1997.

Kimura, F., and T. Kuwagata, Thermally induced wind passing from plain to basin over a mountain range, *J. Appl. Meteorol., 32,* 1538-1547, 1993.

Lauer, W., and D. Klaus, The thermal circulation of the central Mexican meseta region within influence of the trade winds, *Arch. Meteorol. Geophys. Bioklimatol., 23,* 343-366, 1975.

Legg, B. J., and M. R. Raupach, Markov-chain simulation of particle dispersion in inhomogeneous flows: The mean drift velocity induced by a gradient in Eulerian velocity variance, *Boundary Layer Meteorol., 24,* 3-13, 1982.

Louis, J. F., A parametric model of vertical eddy fluxes in the atmosphere, *Boundary Layer Meteorol., 17,* 187-202, 1979.

Lu, R., and R. P. Turco, Air pollutant transport in a coastal environment, I, Two-dimensional simulations of the sea-breeze and mountain effects, *J. Atmos. Sci., 51,* 2285-2308, 1994.

Mellor, G. L., and T. Yamada, Development of a turbulent closure model for geophysical fluid problems, *Rev. Geophys., 20,* 851-875, 1982.

Nickerson, E. C., G. Sosa, H. Hochstein, P. McCaslin, W. Luke, and A. Schanot, Project AGUILA: In situ measurements of Mexico City air pollution by a research aircraft, *Atmos. Environ., Part B, 26,* 445-452, 1992.

Nickerson, E. C., P. McCaslin, E. Sandoval, V. H. Páramo, and R. Gonzáles, Aircraft observations of ozone, carbon monoxide, and NO_x over Mexico City during project AGUILA, paper presented at International Conference on Air Pollution, Computational Mechanics Publ., Monterrey, Mexico, Feb. 23-25, 1993.

Pielke, R. A., et al., A comprehensive meteorological modeling system: RAMS, *Meteorol. Atmos. Phys., 49,* 69-91, 1992.

Raga, G. B., and L. Le Moyne, On the nature of air pollution dynamics in Mexico City, I, Nonlinear analysis, *Atmos. Envion., 30,* 3987-3993, 1996.

Streit, G. E., and F. Guzmán, Mexico City air quality: Progress of an international collaborative project to define air quality management options, *Atmos. Environ., 30,* 723-733, 1996.

Weber, B. L., and D. B. Wuertz, Comparison of rawinsonde and wind profiler radar measurements, *J. Atmos. Oceanic Technol., 7,* 157-174, 1990.

Wellens, A., N. Moussiopoulos, and P. Sahm, Comparisons of a diagnostic model and MEMO progrognostic model to calculate wind fields in Mexico City, paper presented at Second International Conference on Air Pollution, Computational Mechanics Publ., Barcelona, Spain, Sept. 27-28, 1994.

Williams, M. D., M. J. Brown, X. Cruz, G. Sosa, and G. Streit, Development and testing of meteorology and air dispersion models for Mexico City, *Atmos. Environ., 29,* 2929-2960, 1995.

Zhong S., J. D. Fast, and J. C. Doran, Boundary layer processes within the Mexico City basin and their impact on spatial ozone patterns, 1, Meteorological analyses and simulations, paper presented at 12th Symposium on Boundary Layers and Turbulence, Am. Meteorol. Soc., Vancouver, B. C., Canada, July 28 to Aug. 1, 1997.

J. D. Fast and S. Zhong, Environmental and Health Sciences Division, Pacific Northwest National Laboratory, P.O. Box 999, MSIN K9-30, Richland, WA 99352. (e-mail: jerome.fast@pnl.gov; shiyuan.zhong@pnl.gov)

(Received January 15, 1998; revised April 14, 1998; accepted May 20, 1998.)